SLAC-450
SLAC/SSRL-0089

A PHOTOEMISSION STUDY OF THE DIAMOND AND THE SINGLE CRYSTAL C_{60}

Jin Wu

SLAC-Report-450
March 1994

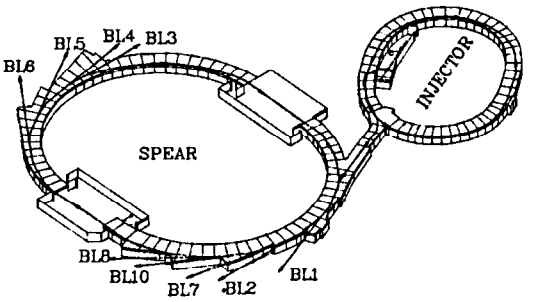

Prepared for the Department of Energy
under contract number DE-AC03-76SF00515

STANFORD LINEAR ACCELERATOR CENTER
STANFORD SYNCHROTRON RADIATION LABORATORY
Stanford University • Stanford, California

SLAC-450
SLAC/SSRL-0089
UC-404
(SSRL-M)

A PHOTOEMISSION STUDY OF THE DIAMOND AND THE SINGLE CRYSTAL C_{60}

Jin Wu

Stanford Linear Accelerator Center
Stanford Synchrotron Radiation Laboratory
Stanford University, Stanford, California 94309

March 1994

Prepared for the Department of Energy under contract number DE-AC03-76SF00515

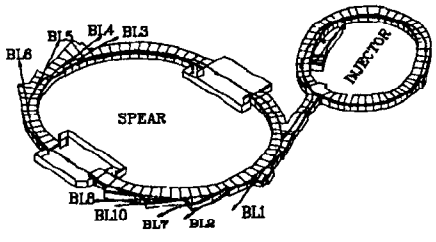

Printed in the United States of America. Available from the National Technical Information Service, U.S. Department of Commerce, 5285 Port Royal Road, Springfield, Virginia 22161

* Ph.D. thesis

ABSTRACT

In the last few years the interest in the properties and applications of the novel forms of carbon, diamond and C_{60}, has exploded. Semiconducting diamond is becoming a material of major interest and importance for application in high temperature and high power electronic devices. The newly discovered C_{60} molecule has showed an entire range of interesting properties and promising practical applications. The understanding of the surface properties of these materials is essential for all the applications.

This work contains two parts. The first is the photoemission study of the natural diamond (100) surface and metal/diamond interface, the second part is the study of the single crystal buckyball.

In the first part, we have studied the electronic structure of diamond (100) surface using photoelectron spectroscopy and low energy electron diffraction for the first time. A surface-related shift has been observed in the C 1s core level spectrum. The surface-state band dispersion was measured along the symmetry axis Γ-J' in the surface Brillouin zone. For $\mathbf{k}_{\parallel} = 0$, there is a very pronounced surface state 1.5 eV below Fermi level E_F, and it disperses downwards with increasing $\mathbf{k}_{\parallel}$. Near the boundary of the surface Brillouin zone J', we find two states with binding energies of 1.9 and 2.4 eV with respect to E_F.

In the fabrication process of diamond electronic devices, doping of diamond and understanding of diamond/metal interfaces are important. We have also studied the boron/diamond and antimony/diamond interfaces. As a Column III element, boron is a possible p-type dopant for diamond. On the other hand, antimony is a possible n-type dopant as a Column V element. Furthermore, boron-doped CVD diamonds have been

grown in several laboratories. In addition, B and Sb play an important role in Si and Ge heteroepitaxial growth. On the Si(100) surface, epitaxial growth of Si and Ge layers has been achieved on top of the B/Si(100)-(2×1) surface at relatively low temperatures. While on the Si or Ge surface one ordered monolayer of Sb occupies the epitaxial sites and saturates the surface dangling bonds, which leads to uniform epitaxial growth. Although diamond has the same crystal structure as both silicon and germanium, it has a drastically smaller lattice and much stronger bond. This makes it very difficult to extrapolate the behaviors of boron and antimony on diamond from its behavior on either silicon or germanium. In this work, we have studied the electronic and geometric structure of B and Sb on diamond surfaces using photoelectron spectroscopy and low energy electron diffraction. Unlike silicon, we find that no ordered layer of boron forms on diamond, and that boron behaves differently on the C(100) surface as compared to the C(111) surface although the exact adsorption sites could not be determined. We also find that boron diffuses into the substrate after high temperature annealing. Moreover, we also find that antimony strongly bonds to the diamond surface, and that antimony behaves very differently on the C(100) surface as compared to the C(111) surface. Further, we also find that the Sb/diamond system does not behave like antimony on either silicon or germanium. We attribute these results to the drastically smaller diamond lattice and the stronger C-C bond.

In the second part, we report angle-resolved photoemission data from single crystals of C_{60} cleaved in UHV. Unlike the other forms of pure carbon, the valence band spectrum of C_{60} consists of many sharp features that can be essentially accounted for by the quantum chemical calculations describing individual molecules. This suggests that the electronic structure of solid C_{60} is mainly determined by the bonding interactions within the individual molecules. We also observe remarkable intensity modulations of the photoemission features as a function of photon energy, suggesting

strong final state effects. Finally, we address the issue of the bandwidth of the highest occupied molecular orbital (HOMO) state of C_{60}. We assert that the width of the photoemission peak of C_{60} does not reflect the intrinsic bandwidth because it is broadened by the non 0-0 transitions via Franck-Condon principle. Our view point provides a possible reconciliation between the photoemission data and that measured by different techniques.

ACKNOWLEDGEMENTS

My advisor, Prof. Ingolf Lindau, deserves the warmest thanks for providing guidance and encouragement over the years. My thanks also go to Prof. Piero Pianetta for his support. I would also like to thank Dr. Pate for his guidance in my early years at Stanford.

I owe more than I can say to Dr. R. Cao and Prof. Z.-X. Shen, for their guidance and cooperation at various stages of this work, and for their friendship. With their help. I learned how to work independently during SSRL runs, how to present my data and how to write proper scientific papers. It's a unforgettable experience for me to work with them.

I have been very happy and privileged to be associated with the many members of Pianetta and Spicer research group, both past and present. Xiaoyu Yang, Matt Richter, Jeff Terry, Chounyong Kim, Stephanie Yashikawa, Lawrence Pan, Paul King, Fred Coffman, Dave King, Dan Dessau, Berry Wells, Dan Marshell and Al Green have been a wonderful source of both friendship and useful technical interactions.

I would also like to acknowledge Ron Morris and George Husek for their technical support. They did a lot excellent machine work, sometimes even did the work during their lunch hours. I am grateful to Magret Kinsella, Gloria Barnes and many SSRL stuff for their supports.

Finally, I would attempt the impossible task of expressing my gratitude to my family. My father and mother, Guodong Wu and Lily Wang, and my brother have provided the loving and encouraging environment over the years which has been the foundation of my successful completion of graduate school.

This research was performed at the Stanford Synchrotron Radiation Laboratory (SSRL) which is operated by the Department of Energy, Office of Basic Energy Sciences, Divisions of Chemical Sciences. The Office's Division of Materials Sciences has provided support for this research.

To my parents, Lily Wang and Guodong Wu

my Husband, Ming Xie

and my son, Sagi

CONTENTS

LIST OF FIGURES

Chapter 1

Introduction

1.1 Motivation

In the last few years the interest in the properties and applications of the novel forms of carbon, synthetic diamond and C_{60}, has exploded. *Science* magazine named diamond and C_{60} "the molecule of the year" in 1990 [1] and 1991 [2], respectively, a distinction which reflects the recent rapid advances in synthesizing diamond under metastable conditions and the new discovery of a third basic form of carbon, C_{60}, buckminsterfullerene.

The carbon atom has been the most intensely studied of all the elements. For centuries we believed the element carbon existed in only two basic, allotropic, and well known forms: diamond and graphite. In hard, sparkling diamond, the carbon atoms are arranged in little pyramids, while soft, dull, slippery graphite consists of sheets of carbon atom hexagons. Research has now confirmed the existence of a third previously unknown form — buckminsterfullerene (C_{60}, also known as buckyball) and its relatives, the fullerenes . The C_{60} molecule has a highly unusual structure, in which sixty carbon atoms are joined together as a cage consisting of twenty hexagons and twelve pentagons in the form of a soccer ball. Both diamond and C_{60} have some unique characteristics that have opened a broad range of applications, and the research in those fields is being pushed forward on many fronts.

One field that this research is taking is the synthesizing of diamond films under metastable conditions. The research in this field has continued to advance very rapidly. The material can be deposited as a film on various substrates with reasonable growth rates [3,4]. Diamond films are commonly applied in the manufacture of cutting tools, wear-resistant parts, heat sinks, and in the development of inert optical coatings, and electronic devices. The materials properties of the diamond thin films are already of the quality to assure a strong market impact in a number of fields. Estimates of the diamond market range from $700 million as a coating only by 1997 to $16 billion by the late 90's overall. The most advanced material requirements will probably be for optical or semiconducting applications, for which we need to know not only how to grow the single crystals but also how to dope the material. Some aspects of device performance have been analyzed recently, and transistor devices have been demonstrated in diamond and epitaxial diamond films grown on diamond.

Another field that the research is taking is the study of the buckyball. As the youngest in the family of the pure carbon solids, the highly symmetric C_{60} molecule has showed an entire range of interesting properties and promising practical applications, that are different from those of either diamond or graphite. For example, chemists learned that C_{60} reacts with alkali metals such as potassium and rubidium, and that it absorbs dozens of these reactive chemical species; physicists found high-temperature superconductivity in alkali doped C_{60}, and observed a large non-linear optical response in C_{60}. Although the buckyball's practical applications have so far been limited by cost, researchers have already found by that coating a Si substrate with C_{70} the growth rate of a diamond film is increased by 10 orders of magnitude over that on untreated silicon.

This work contains two parts. The first, Chapters 2 and 3, is the surface study of natural diamond the and interface study of metal/diamond systems, the second part,

Chapter 4, is the photoemission study of the single crystal buckyball, which is a molecular crystal.

The study of surfaces is an important field of condensed matter research. The interest in the atomic and associated electronic properties of the surfaces arises from both technological implications and basic surface science. The direct technological implications of the study of the diamond surface include metallic adhesion to diamond and diamond film synthesis. The first part of this work has focused on understanding the basic electronic structure of the diamond C(100) surface byangle-resolved photoemission study and a comparison with what is known of other column IV semiconductor surfaces.

The focus of the second part of this study is the understanding of the electronic structure of the single crystal C_{60} and its bandwidth. The newly discovered single crystal C_{60} is a molecular crystal in the face-centered-cubic (FCC) or hexagonal close-packed (HCP) structure. Understanding the electronic structure of the C_{60} single crystal is essential for an understanding of the special properties of this material.

1.2 Background

1.2.1 Classification of Diamond

Scientists divide the natural diamond into four major types according to its optical properties. Type I diamond has a secondary absorption edge at approximately 3200 Å in the ultraviolet absorption spectrum, where the types Ia and Ib can be distinguished in that the Ia diamonds contain aggregated nitrogen that are not magnetic, while the Ib diamonds contain subsitutional nitrogen and are paramagnetic

thus their concentration can be determined by electron spin resonance. These diamonds absorb strongly in the ultra-violet and the absorption extends into the visible region giving the diamonds a characteristic yellow colour. The majority of natural diamonds belong to type Ia, while type Ib diamonds are rare in nature. Most of Ib diamonds are synthetic diamonds formed by high temperature and pressure. Type II diamonds contain less nitrogen, and have the higher conductivities. Their absorption edge extends up to 2300 Å while the type IIa diamonds are insulators, and type IIb are semiconductors. Type IIb are generally p-type, and naturally doped with boron. However, the classification is based on the bulk properties of the diamonds, and no important differences have been found in the surface properties of the four major diamond types. All of the work reported in Chapter 2 and 3 was performed on natural Type II diamonds.

In addition to the traditional classification of bulk single crystal diamonds, polycrystalline diamond films are now produced by chemical vapor deposition at growth rates as high as 1 mm per hour. Today diamond films can be deposited on a number of substrate materials, including metals, ceramics and single crystals of diamond, silicon, sapphire, and graphite. A large supply of hydrogen gas is needed during all diamond growth processes. As a crude estimate, approximately 5000 molecules of H_2 are disassociated for each carbon atom converted to diamond [3]. Although no definitive picture has been formulated for the explanation of the growth mechanism, it is generally believed that atomic hydrogen prevents reconstruction of the diamond surface and suppresses the formation of graphitic nuclei, which allow diamond to form under these metastable conditions.

1.2.2 Classification of the Diamond C(100) Surface

An ideal truncation of the bulk diamond is not energetically favorable. During the creation of the surface, directional covalent bonds must be broken, and the electron

orbitals associated with these broken or dangling bonds are only partially occupied for the truncated bulk diamond, which result in a C(100) surface with two dangling bonds on each diamond surface atom. This energetically unstable situation may be resolved by the saturation of the dangling bond charge density in two ways. The real C(100) surface is either terminated by foreign atoms, in other words, new bonds form at the surface between surface atoms and adsorbates, or reconstructed by a rearrangement of the surface atoms. In other words, new bonds form at surface between surface atoms, resulting in a surface unit cell which is smaller than an ideal surface. A constraint on such relaxations, however, is that there is a limited amount of local surface and subsurface strain that can be accommodated. The final minimum-energy structure, therefore, is the result of a balancing between energy stabilization via reduction of dangling bonds, and energy destabilization resulting from reconstruction-induced local strain fields.

The first way of reducing the surface energy is termination of the lattice by foreign atoms. Experimentally, the mechanically polished C(100) surface was found terminated by hydrogen [5] and (1×1) LEED patterns have been observed. Furthermore, nuclear reaction analysis of polished diamond C(100) surfaces shows that the largest observed hydrogen surface coverage corresponds to two hydrogen atoms per surface carbon atom [6]. Thus, the dihydride structure, i.e. two hydrogen atoms bonding to each of the surface carbon atom is the most favorite model for the (1×1) structure.

The second way of reaching an energetically stable situation is reconstruction. Annealing the surface in ultrahigh vacuum for 5-10 minutes at 1100°C induces the desorption of hydrogen, and transforms the surface into a (2×1) reconstruction [7, 8]. The actual LEED pattern corresponds to a two-domain 2×1 reconstruction with the two domains at 90° to each other. The two different domains are located on terraces

separated by atomic steps. Theoretically, the symmetric dimer structures with either monohydride or π bonding are predicted for the C(100)-(2×1) surface reconstruction [9, 10]. Both of these possible reconstructed structures are shown schematically in Fig 1-1.

For comparison, the behavior of the silicon and germanium surfaces are also briefly reviewed, because silicon and germanium have the same bulk structure as diamond, and they are in the same column of the periodic table. The silicon (100) surface has been studied extensively. Different experiments, such as vibrational spectroscopy, ultraviolet photoelectron spectroscopy, and LEED, have shown that the Si(100)-(1×1) surface is predominantly dihydride terminated. A (2×1) reconstruction on the Si(100) surface was also observed in LEED studies [11-14]. Higher order LEED patterns on the Si(100) surface, such as (2×2) and (4×2) [15-16], have also been observed. Scanning tunneling microscopy (STM) provided the most direct information about the geometric structure [17-20]. These studies showed the existence of dimers, predominantly symmetric as well as asymmetric. Besides a dominating two-domain Si(100)-(2×1) reconstruction, regions of (2×2) and (4×2) periodicity were also observed. It is now generally agreed that the dimer unit is the basic building block of the Si(100) reconstructions. The model for the Si(100)-(2×1) surface, however, is still an open question. Although the STM studies showed that this (2×1) surface is predominantly symmetric dimers, which early theoretical studies [21-22] indicated are metallic and more stable, photoemission studies [23-28] showed that the clean (2×1) surface is semiconducting, which is in accord with buckled dimers [29].

Similar reconstructions are reported for the Ge(100) surface. STM images showed that the clean Ge(100) surface exhibits both symmetric and asymmetric dimers. In high resolution images, most dimers are found to be asymmetric, which is attributed to a buckling of the dimer pairs [30]. Total energy calculations [31] found

that an asymmetric dimer model has the lowest energy for the clean Ge(100)-(2×1) surface.

1.3 Photoemission Spectroscopy

Photoemission spectroscopy (PES) is the main experimental technique used in this work. With its capabilities enhanced by synchrotron radiation, PES has been established as a very powerful tool for studying surface and bulk electronic structures. Different aspects of photoemission spectroscopy have been well-documented in review articles [31- 40]. In this study, different versions of PES are used. They are: (1) angle-resolved photoemission spectroscopy (ARPES); (2) measurement of an energy distribution curve (EDC); (3) x-ray photoemission spectroscopy (XPS); and (4) constant initial-state spectroscopy (CIS).

In a PES experiment, monochromatic photons are incident upon a sample and the kinetic energy of photoemitted electrons is measured by an electron energy analyzer. Figure 1-2 shows a schematic representation of the photoemission process, in which electrons from occupied initial states with energy E_i are excited by the photon into unoccupied final states with energy E_f above the Fermi level. If these states are above the vacuum level, then these electrons may escape from the sample to be detected by an electron energy analyzer. In most cases, the PES process for a sample in the form of a solid can be interpreted by the three-step model [41] in which it is assumed that optical transitions giving rise to the observed photoelectrons are the same as those which give rise to the bulk optical absorption. The optical transition between the initial and the final state is governed by energy conservation

$$E_f(\mathbf{k})-E_i(\mathbf{k})-h\nu=0 \qquad (1.1)$$

One of the ways to perform the photoemission study is angle-resolved photoemission (ARPES). The key features of ARPES are: (1) it can probe both the energy and momentum of electron states in the material simultaneously; (2) it is very sensitive to the electronic environment; (3) it is very surface sensitive, the minimum probing depth is only around 5 Å. However, the main limitation of this technique is that only the component of the photoelectron's momentum parallel to the surface ($\mathbf{k}_{||}$) is conserved as it passes through the surface. In the following, a simple description of ARPES is given.

Angle-resolved photoemission has become an important tool for studies of surface electronic structure. Figure 1-3 shows the geometry of the experimental set-up for ARPES, in which electrons are excited from occupied initial states $E_i(\mathbf{k}_i)$ into final states $E_f(\mathbf{k}_f)$by the photons of energy ($h\nu$). In the conceptually simple three-step [41] model of photoemission from solids, the photoemission process is approximated into that the photoelectrons are first excited, then transported to the surface and finally transmitted through the surface. In a one-electron band model, the electronic states in a crystalline solid are characterized by the electron energy E and the Bloch wavevector **k**. The energy conservation in the optical transitions gives the Eq.(1.1), and momentum conservation gives the following equation:

$$\mathbf{k}_f=\mathbf{k}_f+\mathbf{q}_p=\mathbf{k}_f \qquad (1.2)$$

In ARPES experiments, the photon energy ($h\nu < 50$ eV) is low so that the wavevector of the photon is negligible. If the final-state energy is large enough, and considering

primary unscattered photoelectrons only, the electron can be emitted into the vacuum with a kinetic energy E_k and a corresponding wavevector $\mathbf{k}_k$. We have

$$E_i = E_i + h\nu - \phi \tag{1.3}$$

$$k_i = \frac{\sqrt{2mE_k}}{\hbar} \tag{1.4}$$

Only the component of k parallel to the surface is conserved when an electron goes from the interior of the crystal through the surface into the vacuum. The expression for the parallel wavevector, $k_{||}$, is

$$k_{||} = \frac{\sqrt{2mE_k}}{\hbar} \sin\theta_e \tag{1.5}$$

By measuring the kinetic energy, E_k,of electrons giving rise to a characteristic photoemission feature as a function of emission angle, θ_e, we can obtain a dispersion curve $E_i(k_{||})$. For two-dimensional lattices the band dispersion is only a function of $k_{||}$ and the unknown change in the vertical component $k_\perp$ is of little importance in the analysis of the energy distribution curves. For a surface state band, the dispersion curve obtained is independent of photon energy and the ARPES experiment maps out the E_i vs. $k_{||}$ relation.

More sophisticated theoretical descriptions of the photoemission are the one-step quantum-mechanical models, in which inelastic scattering and the lifetimes of electron and hole are taken into account. An important outcome of those refined models is the introduction of mechanism for broadening in the photoemission spectra. For more details of those models and their applications, see references [43-45].

In addition to ARPES, EDC and CIS modes are also used in this work. In the EDC mode, the number of electrons at a certain kinetic energy for a constant photon

energy gives joint information on the initial- and final-state densities of states. In the CIS mode, the acceptance energy of the analyzer is swept synchronously with photon energy so that the cross section of a particular initial state is monitored as a continuous function of the photon energy.

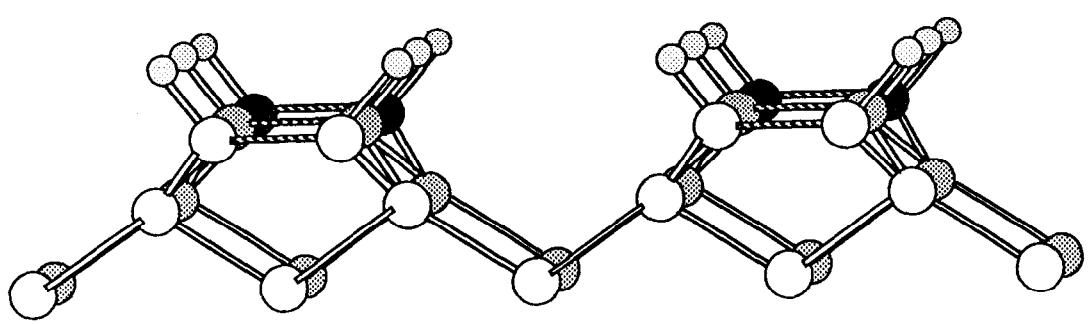

Figure 1-1a Schematic indication of the monohydride model for the C(100)-(2 × 1) reconstruction.

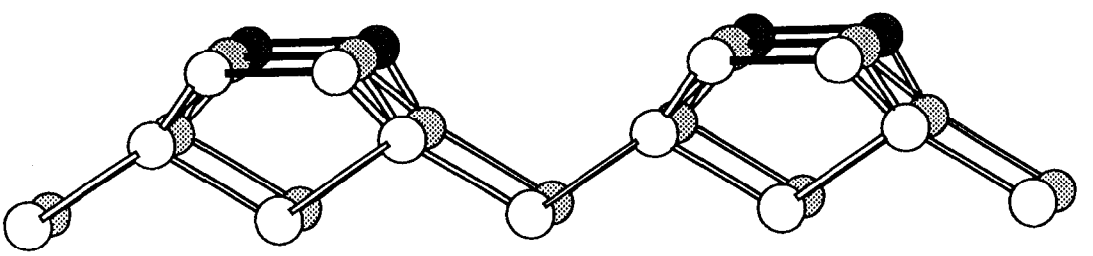

Figure 1-1b Schematic indication of the symmetric-dimer model for the C(100)-(2×1) reconstruction.

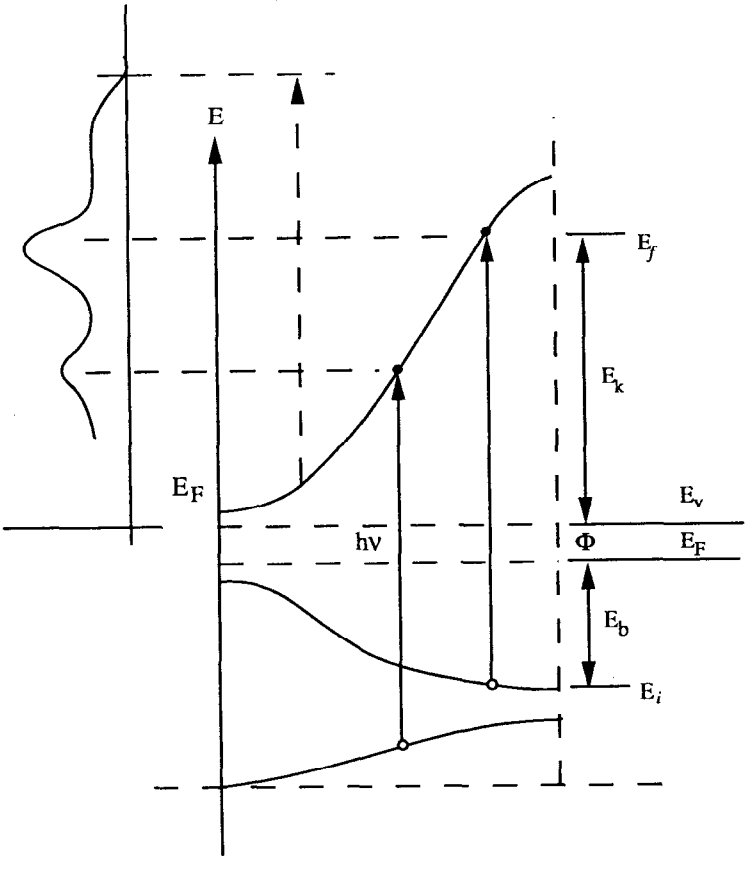

Figure 1-2 A schematic representation of the photoemission process.

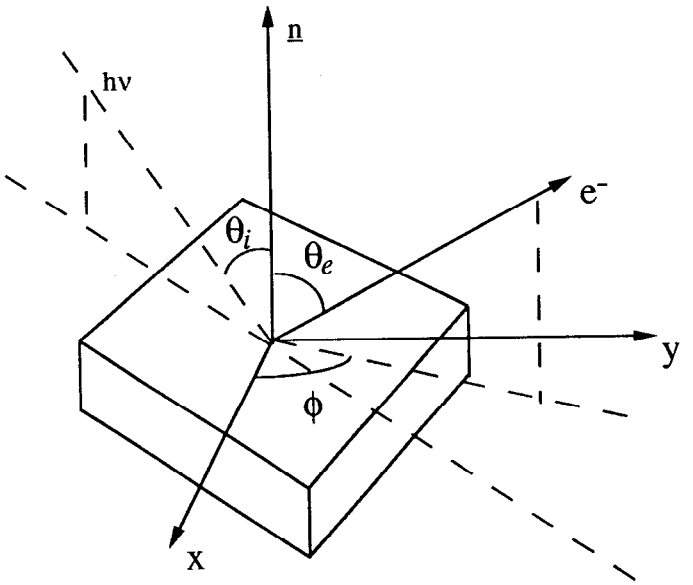

Figure 1-3 The geometry of the experimental set-up for ARPES.

References:

1. D. E. Koshland, Jr. Science **250**, 1637 (1990).
2. Science, **254**, 1534 (1991).
3. J. C. Angus, Y. Wang and M. Sunkara, Annu. Res. Mater. Sci. **21**, 221 (1991).
4. R. J. Nemanich, Annu. Res. Mater. Sci. **21**, 535 (1991).
5. B. B. Pate, Ph.D. Thesis, Stanford University, 1984.
6. T. E. Derry, C. C. P. Madiba and J. P. F. Sellschop, Nucl. Instrum. Methods **218**, 559 (1983).
7. P. G. Lurie and J. M. Wilson, Surf. Sci. **65**, 453 (1977).
8. P. G. Lurie and J. M. Wilson, Surf. Sci. **65**, 476 (1977).
9. W.S Verwoerd, Surf. Sci. **103**, 404 (1981).
10. X. M. Zheng and P. V. Smith, Surf. Sci. **256**, 1 (1991).
11. R. E. Schlier and H. E. Farnsworth, J. Chem. Phys. **37**, 729 (1959).
12. W. S. Yang, F. Jona and P. M. Marcus, Solid State Commun. **43**, 847 (1982).
13. W. S. Yang, F. Jona and P. M. Marcus, Phys. Rev. B **28**, 2049 (1983).
14. B. W. Holland, C. B. Duke and A. Paton, in: Proc. 17th Int. Conf. on the Physics of Semiconductors, Eds. D. J. Chadi and W. A. Harrison, Springer, Berlin, p. 59 (1984).
15. M. J. Cardillo and G. E. Becker, Phys. Rev. Lett. **40**, 1148 (1978).
16. M. J. Cardillo and G. E. Becker, Phys. Rev. B **21**, 1497 (1980).
17. R. M. Tromp, R. J. Hampers and J. E. Demuth, Phys. Rev. Lett. **55**, 1303 (1985).
18. R. J. Hampers, R. M. Tromp and J. E. Demuth, Phys. Rev. B **34**, 5343 (1986).
19. R. J. Hampers and U. K. Kohler, Surf. Sci. **181**, 346 (1987).
20. R. J. Hampers and U. K. Köhler, J. Vac. Sci. Technol. A **7**, 2854 (1989).

21. J. A. Applebaum, G. A. Baraff and D. R. Hamann, Phys. Rev. B **12**, 5749 (1975).

22. G. P. Kerker, S. G. Louie and M. L. Cohen, Phys. Rev. B **17**, 706 (1978).

23. F. J. Himpsel and D. E. Eastman, J. Vac. Sci. Technol. **16**, 1302 (1979).

24. R. I. G. Uhrberg, G. V. Hansson, J. M. Nicholls and S. A. Flodström, Phys. Rev. B **24**, 4684 (1981).

25. R. D. Bringans, R. I. G. Uhrberg, M. A. Olmstead and R. Z. Bachrach, Phys. Rev. B **34**, 7447 (1986).

26. F. J. Himpsel and T. Fauster, J. Vac. Sci. Technol. A **2**, 814 (1984).

27. P. Martensson, A. Cricenti and G. V. Hansson, Phys. Rev, B **33**, 8855 (1986).

28. A. L. Wachs, T Miller, T. C. Hsieh, A. P. Shapiro and T. C. Chang, Phys. Rev. B **32**, 2326 (1985).

29. P. Krüger, A. Mazur, J. Pollman and G. Wolfgarten, Phys. Rev. Lett. **57**, 1468 (1986).

30. J. A. Kubby, J. E. Griffith, R. S. Becker and J. S. Vickers, Phys. Rev. B **36**, 5543 (1988).

31. J. Pollmann, P. Krüger and A. Mazur, J. Vac. Sci. Technol. B **5**, 945 (1987).

32. Edited by M. Cardona and L. Ley, *Photoemission in Solids I*, Springer-Verlag, New York, 1978.

33. Edited by M. Cardona and L. Ley, *Photoemission in Solids II*, Springer-Verlag, New York, 1979.

34. B. Feuerbacher, B. Fitton and R. F. Willis, *Photoemission and the Electronic Properties of Surfaces*, Wiley, New York, 1978.

35. I. Lindau and W. E. Spicer, *Synchrotron Radiation Research*, Edited by H. Winick and S. Doniach, Plenum, New York, 1980.

36. E. W. Plummer and W. Eberhardt, Advan. Chem. Phys. **49**, 533 (1982).

37. C. O. Almbladh, and L. Hedin, *Handbook on Synchrotron Radiation*, Ed. E. E. Koch, Chap. 8, North-Holland, Amsterdam (1983).

38. N. V. Smith, and F. J. Himpsel, *Handbook on Synchrotron Radiation*, Ed. E. E. Koch, Chap. 9, North-Holland, Amsterdam (1983) .

39. F. J. Himpsel, Advan. Phys. **32**, 1 (1983).

40. F. J. Himpsel and N. V. Smith, Phys. Today **38**, No. 12, 60 (1985).

41. G. V. Hansson and R. I. G. Uhrberg, Surf. Sci. Report **9**, 197 (1988).

42. C. N. Berglund and W. E. Spicer, Phys. Rev. A **136**, 1030 (1964).

43. C. Caroli, D. L. Rozenblatt, B. Roulet, D. S. James, Phys. Rev. B **8**, 4552 (1973).

44. A. Liebsch, Phys. Rev. B **13**, 544 (1976).

45. J. B. Pendry, Surf. Sci. **57**, 679 (1976).

Chapter 2

Electronic Structure of the Diamond (100) Surface

Abstract

The electronic structure of the diamond C(100)-(2 × 1) surface has been investigated by means of core level spectroscopy and angle-resolved photoelectron spectroscopy for the first time. A surface-related shift, 0.95 eV towards lower binding energy, has been observed in the C 1s core level spectrum. The surface-state dispersion in the valence band was measured along the symmetry axis Γ-J' in the surface Brillouin zone. For $\mathbf{k}_{\parallel} = 0$, there is a very pronounced surface state 1.5 eV below Fermi level E_F, which disperses downwards and splits into two states with increasing $\mathbf{k}_{\parallel}$. Near the boundary of the surface Brillouin zone J', we find two states with binding energies of 1.9 and 2.4 eV with respect to E_F.

2.1 Introduction

People recognized the remarkable properties of diamond long ago. The name originates from the Greek *adamas*, which means invincible. Many people are aware of the unusual optical properties of diamond from its wide distribution as a gem stone. Its combination of properties, like its appearance, is absolutely wonderful. Diamond is the hardest substance known. It conducts heat better than any other material, has extremely

high electrical resistance, and is transparent to x-rays and ultraviolet radiation. It is inert to chemical corrosion. Diamond films could be more stable and would remove accumulated heat more rapidly than silicon wafers. Scientifically the material is unique because the diamond crystal structure is prototypical for a semiconductor. Because of these outstanding properties, diamond has great potential both in basic research and in commercial applications.

In recent years, techniques have been developed for depositing polycrystalline diamond films under metastable conditions by the chemical vapor deposition (CVD) on various substrates. In 1990, *Science Magazine* named diamond "the molecule of the year" in recognition of this development [1].

However, the understanding of the diamond growth process is still very poor, which stems, to large extent, from a lack of understanding of the diamond surface electronic structure. Fairly few studies, both theoretical and experimental, have been conducted on diamond surfaces. Among earlier studies, research work was focused on the C(111) surface [2-8] which is relatively easy to prepare. On the C(111) hydrogen-terminated surface, each surface carbon atom bonds to one atomic hydrogen, while the C(100) hydrogen-terminated surface is a dihydride surface. Therefore, a higher annealing temperature is needed to reconstrute the C(100) surface. The current understanding of the C(100) surface is incomplete and controversial, in spite of a few experimental and theoretical investigations over the years [8-11].

In comparison, extensive theoretical and experimental studies have been carried out for Si and Ge [12-16], resulting in tremendous progress in terms of our understanding of these materials and astonishing improvement of the device processing.

In this work, we have studied the surface structure of natural type IIb diamond C(100) using angle-resolved core level and valence band photoemission spectroscopy (ARPES). To best of my knowledge, this work is the first study of this kind on the

C(100) surface. One chemically shifted component in the C 1s core level has been resolved, that is attributed to the surface dimer of the C(100) surface. We have observed two surface related states in the valence band spectra and determined their dispersion along Γ-J' direction in the surface Brillouin zone. These results will be compared with the results obtained from the Si(100) surface, a much better understood surface that has a similar structure to diamond.

2.2 Historic Review

In this section, I will briefly review some important early work on the diamond (100) surface.

In early low-energy electron diffraction (LEED) studies on diamond, Lurie and Wilson [17] reported that the natural C(100) surface is reconstructed and exhibits a superposition of (2×1) and (1×2) LEED patterns after a cleaning treatment, in which the diamond is heated to 1300°C for 5-10 minutes in better than 5×10^{-10} Torr vacuum. They considered the vacancy model of Lander and Morrison [18, 19], and assumed that the presence of surface imperfections is necessary as the source and sink of diffusing carbon atoms. They then proposed that two processes are involved during diamond heating: (i) the removal of alternate rows of surface carbon atoms with their bonded hydrogen atoms plus another two atomic hydrogen atoms from adjacent remaining carbon atoms in the form of methane gas; (ii) the double bonding of the dangling bonds left on the surface to the second layer of carbon atoms. In this way all the dangling bonds are saturated.

On the other hand, Phillips [20, 21] studied vacancies and the reconstruction of covalent surfaces. He commented that heating the diamond at the temperature required

for the creation of vacancies causes carbonization or formation of a graphitic layers, which appears to rule out vacancy models in the case of diamond.

Following these two works, Verwoerd [22, 23] calculated the dimer bond on the reconstructed C(100) surface and the process of hydrogen chemisorption onto the diamond surface by cluster calculations of a 4-layer atomic cluster with a single surface pair. Using the MINDO/MNDO quantum chemistry programs, he predicted that for the C(100) surface, both electron pairs on carbon are engaged in bonding and the symmetric dimer pair is the lowest energy configuration.

Seven years later, in 1988, Bechstedt and Reichardt [24] investigated the dimer reconstruction of (100)-(2x1) surfaces of group IV materials by using the total energy minimization within the self-consistent tight-binding method. They concluded that a slightly asymmetric dimer for both the C(100) and Si(100) surface reconstructions.

In 1990, Hamza, Kubiak and Stulen [25] reported their experimental results on the natural type IIa and IIb diamond C(100) samples. They showed that diamond C(100) reconstructs upon heating to greater than 1027° C, and that the reconstructed surface exhibits a LEED pattern with two domains of (2x1) symmetry. They ruled out the correlated buckled dimers as a possible structure for the reconstruction because they did not observed higher order reconstructions. They studied the role of hydrogen during the reconstruction by monitoring the chemisorbed hydrogen on the diamond surfaces. The technique that they employed is the electron-stimulated desorption time-of-flight spectroscopy (ESD-TOF), in which they found that two distinct H^+ features on the C(100)-(1x1) surface, but on the C(100)-(2x1) surface, the fast feature disappeared, but the slower one remains even after annealing up to 1257°C. In addition, they also observed the occupied surface states in the band gap for C(100)-(2x1) surface. They suggested that symmetric dimers with monohydride termination at each carbon atom of the pair is the most likely structure.

In 1991, Zheng and Smith [11] employed the SLAB-MINDO method in the theoretical study of the C(100) surfaces They also predicted a symmetric dimer structure for both the clean C(100)-(2x1) and the monohydride C(100)-(2x1):H surface reconstructions. After the surface reconstruction, the lowering of the energy is 3.93eV per surface atom.

2.3 Experimental

The photoemission study of C(100) surface was conducted at Stanford Synchrotron Radiation Laboratory on a multi-undulator beam line V-2, which consists of a tunable multiple undulator source and the "Locust" UHV monochromator [26]. In this combination of source and monochromator, the fundamental energy of the undulator output can be tuned to the monochromatic pass energy of the Locust across the full scanning range of the instrument. The beamline is capable of providing photons with high photon flux and very good resolution across an energy range of 10 to 1000 eV. Four different; 10, 15, 24, and 30 period permanent magnet undulators are installed for providing the wide scanning range required for the beamline. The spectral output of the undulator is governed by the magnetic field and the period of the device and the energy of the stored electron beam. The Locust monochromator is descended from the Grasshopper monochromator. Four sets of gratings, with 2, 4, 10 and 20 degrees of incidence angle, are employed in order to accomplish high transmission efficiency over a wide scanning range.

A VG ADES-400 angle resolved ultra high vacuum system that consists of a main chamber housing a low energy electron diffraction (LEED) optics, a hemispherical energy analyzer, and a sample load lock system was used. The sample manipulator was equipped with an azimuthal rotation mechanism and an e-beam heater

for high temperature annealing. The base pressure of the chamber during the experiment was $< 2 \times 10^{-10}$ torr. The angular resolution of the ADES 400 analyzer is ~2° and the overall energy resolution is about 250 meV.

The natural type IIb C(100) surface studied here was mechanically polished on a rotating wheel of cast iron periodically replenished with a mixture of diamond grit and olive oil. During the polishing the grit itself is eroded, and its size at the end of polishing process is believed to be well below 1μm. [4, 27] The olive oil acts as a hydrogen source to terminate the diamond surface, which behaves like a passivation layer for the surface. The sample was then cleaned for UHVconditions, transferred into the experimental chamber through a load lock system and outgassed at 500°C until the chamber pressure recovered close to the base pressure. We found that the hydrogen terminated diamond surface is very stable even at a temperature of ~800°C. The clean C(100) surface was finally created by annealing the sample at ~1100°C for 10 minutes yielding a (2 × 1) LEED pattern. Another experimental concern is the possible charge accumulation on the sample during the photoemission process since diamond is a wide band gap semiconductor with a band gap of 5.5 eV. But a previous study [4] has indicated that sample charging would not become a serious problem during the photoemission study as long as the edge of the sample surface had a good electrical contact to ground.

2.3 Results and Discussion

The ideal bulk-like C(100) surface is shown in Figure 2-1. The bulk-truncated C(100) surface leaves two dangling bonds for each surface carbon atom. As polished, both of these dangling bonds are saturated by hydrogen, as shown in Figure 2-2.

In Figure 2-3 we present the C 1s core level spectra for the hydrogen terminated and reconstructed clean diamond (100) surfaces at normal emission. For the hydrogen terminated diamond surface that has been annealed at 800°C, the computer least-square fitting indicates that the spectrum consists of a single component. The (1 × 1) LEED pattern implies that this surface has the same type of geometrical structure as the unreconstructed truncated diamond. Both the PES and LEED results reflect that the top layer carbon atoms are in the very similar enviroment to that of bulk atoms, although two bonds of the top carbon atom are bonded to hydrogen. When this hydrogen terminated surface is annealed at 1100°C, rather drastic changes take place in both the LEED pattern and PES spectrum. The (1 × 1) LEED pattern is replaced by a (2 × 1) pattern and the C 1s core level spectrum now contains two components. The separation between the two components is about 0.93 eV. One of the component is contributed by the bulk atoms, the other is contributed by atoms of the top layer. The question need to be answered is which component is related to the surface atoms. We have determined that the lower binding energy component originates from the diamond surface by varying the probing depth, which can be achieved by either changing the incident photon energy or the emission angle of the photoelectrons. Figure 2-4 shows the C 1s spectrum from the reconstructed C(100) (2 × 1) surface at 40° emission angle. At this emission angle, the photo-electrons generated at the same depth have to travel longer distance inside the solid than those emitted at surface normal, so that the effective escaping depth is smaller than that at normal emission. In the other words, at 40° emission angle the surface related component is enhenced. which is the component at lower binding energy side.

As with the other group-IV semiconductors, an ideal truncation of the bulk diamond would result in a (100) surface with two dangling bonds on each surface carbon atom. This situation is not energetically favorable. A rearrangement of the surface atoms to lower the surface energy then takes place, resulting in a surface unit

cell which is larger than that for the ideal surface and with fewer dangling bonds. That is exactly what has been observed here for the diamond with a (2×1) reconstruction. In this case, the surface carbon atoms are in a different electronic environment compared with the bulk carbon atoms. This is reflected by the chemically shifted component in the C 1s core level spectrum for the reconstructed diamond (100) surface. The surface core level components have also been observed for other group IV semiconductors [2, 29-32]. For the hydrogen terminated diamond surface, all the dangling bonds are believed to be saturated by hydrogen atoms. As a result, the top layer carbon atoms see a rather similar environment as their bulk partners, which is reflected by a single component in the photoemission core level spectrum. We also notice that the line width of the C 1s core level from the H:C surface is about a few tenths eV wider than that from the clean C(100) surface. This may be because for the hydrogen terminated C(100), the top surface carbon atoms still show a small shift that can not be resolved with our energy resolution. The broadening could also come from inhomogeneity of this surface. Finally we have observed a peak shift of the bulk component for the hydrogen terminated diamond with respect to that of the clean diamond surface. This essentially represents the change of the surface band bending of these two surfaces, where the H-C(100) shows 0.55 eV more in band bending.

The atomic arrangment on semiconductor surface has always been an important area and there have been extensive studies [1, 16, 28, 32]. It is generally agreed that the surface Si and Ge atoms tend to form dimers on the clean (100) surfaces. Whether these dimers are symmetric or asymmetric remains to be answered. For C(100) our results are consistent with a recent theoretical study [11] that concludes that it is very likely that the carbon atoms on the C(100) surface will form symmetric dimers. But we must point out that higher resolution must be employed to determine the accuracy of the geometric model.

The clean C(100) surface shows a (2×1) LEED pattern actually corresponding to a two-domain (2×1) reconstruction with the two domains at 90° to each other. The surface Brillouin zones of this surface are illustrated in Figure2-5 showing the superimposed surface Brillouin zones of the two different domains. The ARPES valence band spectra ($h\nu = 40$ eV) of the reconstructed C(100) surface as a function of the photoelectron emission angle taken along [011]/[01$\bar{1}$] directions are presented in Figure 2-6. We have observed two features highlighted by the tic-marks. The energies of these features are referred to the Fermi level (E_F) which was determined from a platinum metal sample. The most pronounced feature, S_1, observed in this set of spectra is the peak located around 1.5 eV below the E_F close to Γ point of the Brillouin zone. We did vary the incident photon energy and saw no dispersion of this state as a function of the photon energy. This indicates that this feature has surface state character. In Figure 2-7 the normal emission valence band spectra for the clean and hydrogen terminated C(100) surface are shown. The spectrum for the hydrogen terminated diamond surface has been shifted by -0.55 eV to correct for the band bending on this surface. Clearly, for the hydrogen covered C(100) surface there is no emission observed from the area near the Fermi level. This further shows that the feature near the Fermi level from the reconstructed C(100) surface originates from the surface state emission. Also, with the help of the valence band spectra taken on a hydrogen terminated C(100) surface, we have determined that all the features with a binding energy of 4 eV or higher originate from bulk contributions.

For the surface state, as we vary the photoelectron emission angle along the [011]/[01$\bar{1}$] directions, dispersion does occur. The dispersion of the surface state is presented in Figure 2-8(a), where their initial energies as a function of the wave vector $E(\mathbf{k}_{\parallel})$ are plotted. The shaded regions are the projected bulk band structure [33]. The main surface state feature, which is a pronounced peak at normal emission, disperses downwards from -1.5 at the zone center to -2.4 eV at the zone boundary at J' (see

Figure 2-6). Additionally, a second peak S_2 at -1.9 eV is seen near the zone boundary at J', which might be degenerate in energy with the main peak seen at Γ. It should be pointed out that since the surface has a mixture of (2 × 1) and (1 × 2) domains, the dispersion shown in Figure 2-8 should also be considered as the combination of the surface state dispersions along both [011] and [01$\bar{1}$] directions. Since theoretical work specific to this diamond surface is not available, we compare our result of the C(100)-(2x1) to the result of the Si(100)-(2x1) surface [29]. Overall, the surface-related features S_1 and S_2 of the C(100) valence band spectra and their dispersion appear to be very similar to those observed on the Si(100) surfaces [12, 29], although the magnitude of dispersion may differ to a certain extent. This apparently stems from the similar structures of the two semiconductors. It should be mentioned that certain surface-related features observed for the Si(100) surface, such as S_3-S_5 [34], have not been detected for the diamond surface. The main reason is probably that those features are usually observable along the [010] direction, while in our case we only investigated the dispersion along the [011] /[01$\bar{1}$] directions. Future careful and systematic studies of the C(100) surface may reveal more features.

2.5 Conclusions

We have studied the electronic structure of reconstructed diamond (100) surface using both core level and angle resolved valence band photoemission spectroscopy for the first time. One surface component of the C 1s core level spectrum is observed, which is in agreement with theoretical calculations that this surface is most likely to consist of only symmetrical dimers. In the valence band spectra we have identified the emission from the surface states and mapped out the dispersion along [011] /[01$\bar{1}$]

directions. The results from this study have been compared to those from the reconstructed Si(100) and Ge(100) surfaces, and we have found that there is a great similarity in the surface electronic structures.

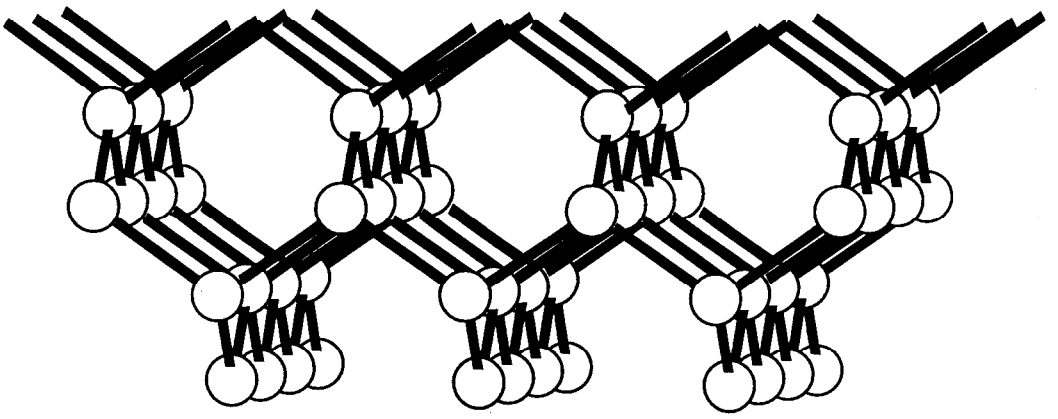

Figure 2-1 Schematicrerepresentation of the ideal bulk-like C(100)-(1 × 1) surface

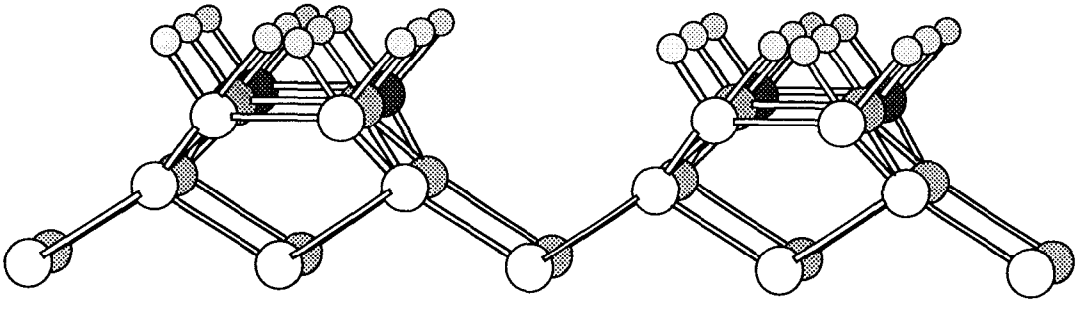

Figure 2-2 Schematic representation of the dihydride model for the H/C(100)-(1 × 1) surface.

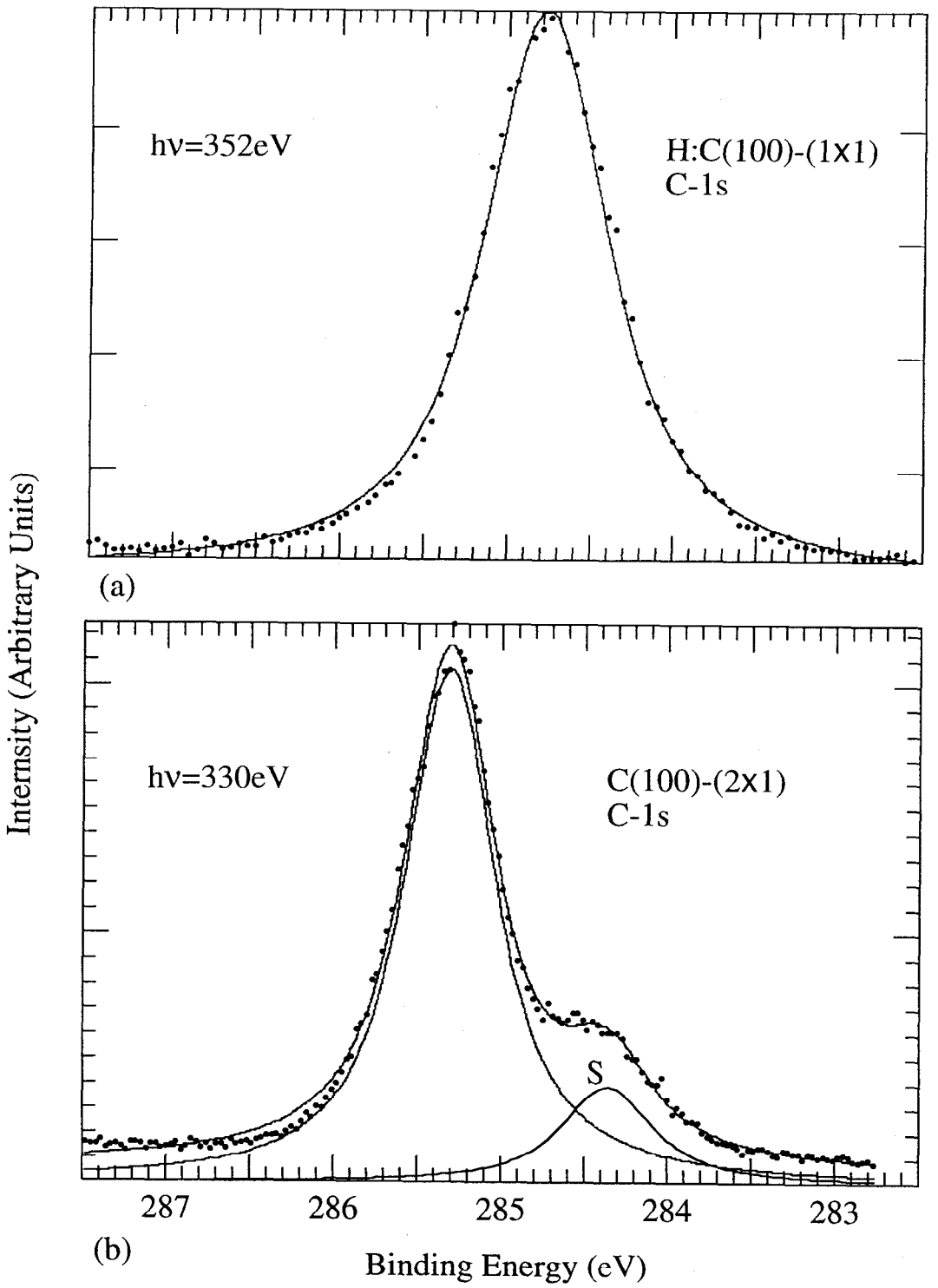

Figure 2-3 C 1s core level spectra from (a) the H/C(100)-(1×1) and (b) the reconstructed C(100)-(2×1) surfaces with the emission angle θ_e= 0°(See Fig. 2-4).

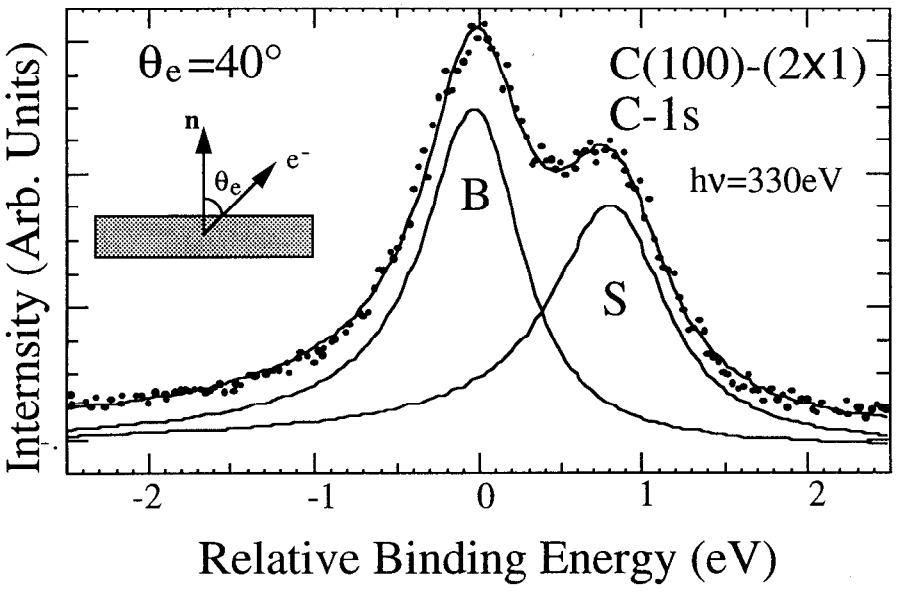

Figure 2-4 C 1s core level spectra from the reconstructed C(100)-(2 × 1) surface with the emission angle θ_e= 40°

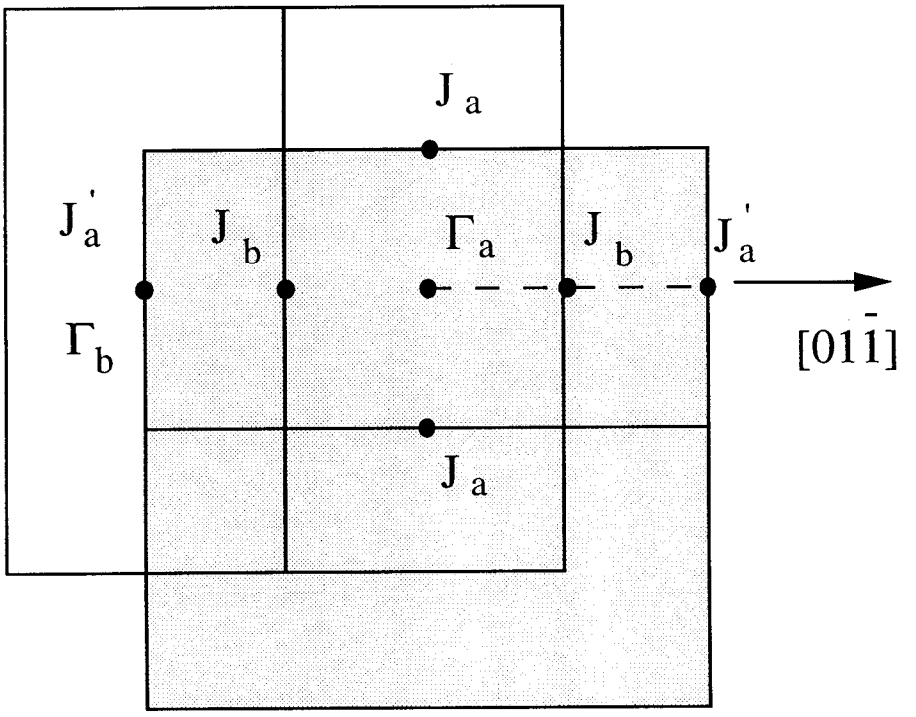

Figure 2-5 Surface Brillouin zones for a two-domain 2x1 reconstruction on C(100).

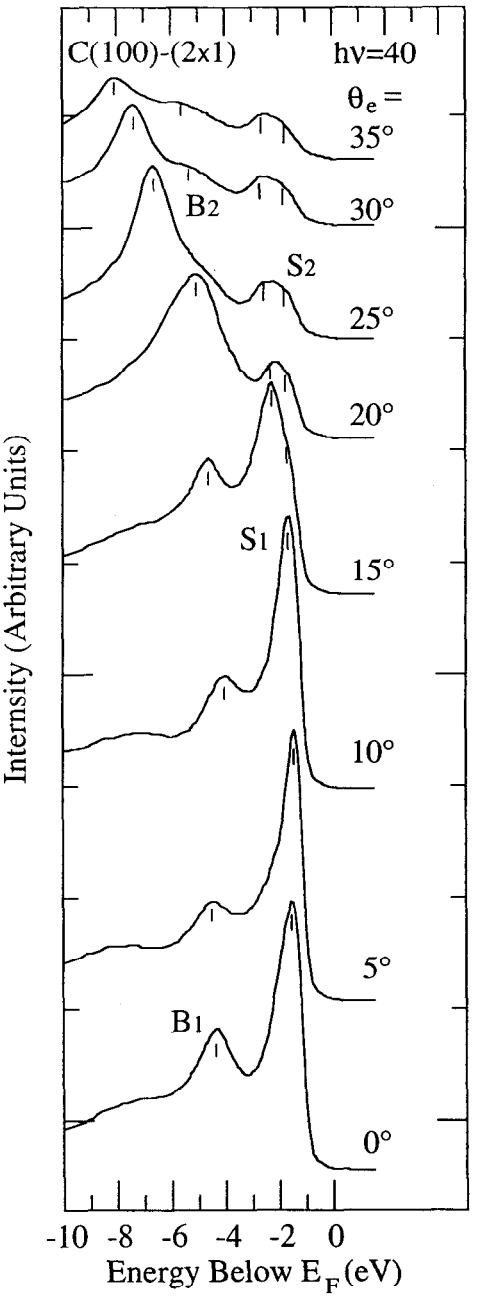

Figure 2-6 An angular series of spectra from the C(100)-(2x1) surface, recorded with 40 eV photon energy and incident angle 45°. Surface features are labeled by S and bulk features are labeled by B.

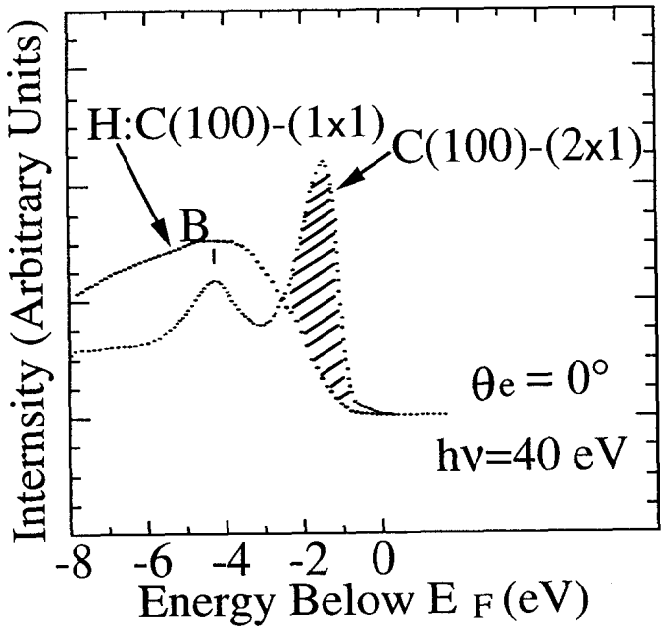

Figure 2-7 ARPES spectra of the C(100)-(2x1) surface showing extra surface state emission near the Fermi energy.

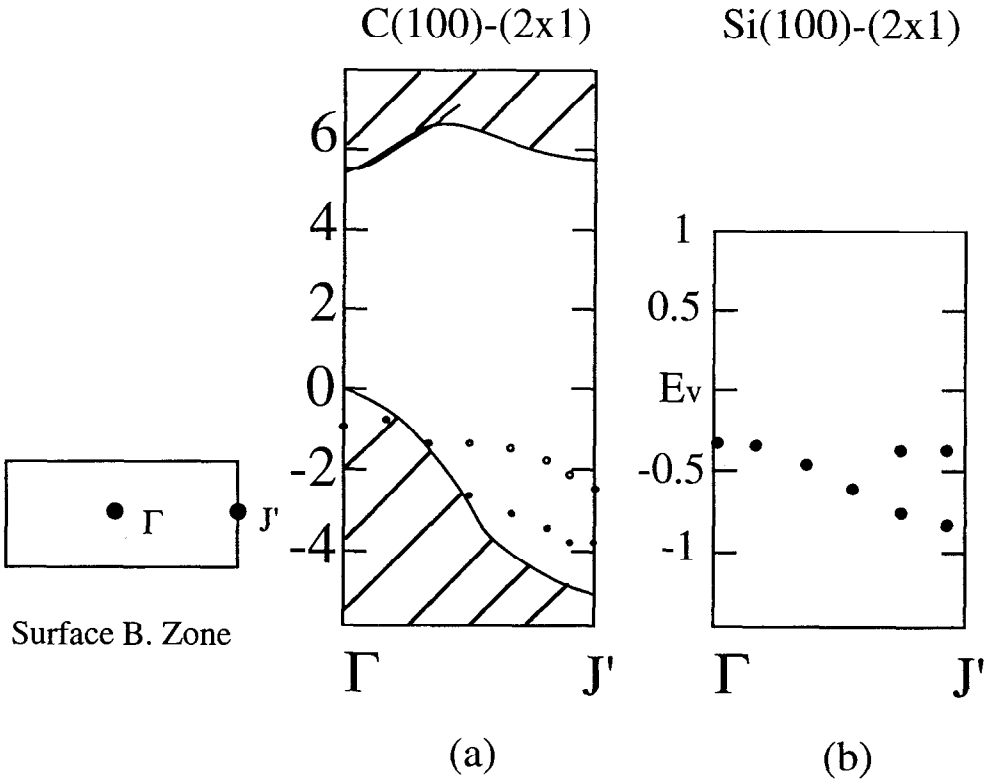

Figure 2-8 (a) Experimental surface state dispersion for C(100)-(2x1) in the ΓJ' direction. Due to the presence of multidomains J_b is a combination point, which is on the boundary of domain B and inside the first zone of domain A (See Figure 2-3). (b) Experimental surface state dispersion for Si(100)-(2x1) in the same direction [29].

References:

1. D. E. Koshland, Jr. Science **250**, 1637 (1990).
2. F. J. Himpsel, D. E. Eastman, P. Heimann and J. F. van der Veen, Phys. Rev. B **24,** 7270 (1981).
3. D. Vanderbilt and S. G. Louie, Phys. Rev. B **30**, 6118 (1984).
4. B. B. Pate, Surf. Sci. **165**, 83 (1986).
5. A. V. Hamza, G. D. Kubiak and R. H. Stulen, Surf. Sci. **206**, L833 (1988).
6. X. M. Zheng and P. V. Smith, Surf. Sci. **253**, 395 (1991).
7. S. Iarlori, G. Galli, F. Gygi, M. Parrinello, and E. Tosatti, Phys. Rev. Lett. **69**, 2947 (1992).
8. P. G. Lurie and J. M. Wilson, Surf. Sci. **65**, 453 (1977).
9. W. S. Verwoerd, Surf. Sci. **108**, 153 (1981).
10. A. V. Hamza, G. D. Kubiak and R. H. Stulen, Surf. Sci. **237**, 35 (1990).
11. X. M. Zheng and P. V. Smith, Surf. Sci. **256**, 1 (1991).
12. G.V. Hansson and R.I.G. Uhrberg, Surf. Sci. Rep. **9**, 197 (1988).
13. F. J. Himpsel, Surf. Sci. Rep. **12**, 1 (1990).
14. D. J. Chadi, surf. Sci. **99** , 1 (1980).
15. R.I.G. Uhrberg and G.V. Hansson, Crit. Rev. solid State Mater. Sci. **17** 133 (1991).
16. J. P. LaFemina, Surf.Sci. Rep. **16,** 133 (1992).
17. P. G. Lurie and J. M. Wilson, Surf. Sci. **65**, 453 (1977) .
18. J.J. Lander and J. Morrison, J. Chem. Phys. **34**, 1403 (1963).
19. J.J. Lander and J. Morrison, Surf. Sci. **4**, 241 (1966).
20. J.C. Phillips, Surf. Sci. **40**, 459 (1973).

21. J. C.. Phillips, Surf. Sci. **53**, 474 (1975).

22. W.S Verwoerd, Surf. Sci. **103**, 404 (1981).

23. W.S Verwoerd, Surf. Sci. **108**, 153 (1981).

24. F. Bechstedt and D. Reichardt, Surf. Sci. **202**, 83 (1988).

25. A. V. Hamza, G. D. Kubiak and R. H. Stulen, Surf. Sci. **237**, 35 (1990).

26. BL-V

27. Grodzinski, *Diamond Technology* (NAG Press, London, 1953).

28. R. Cao, X. Yang, J. Terry, and P. Pianetta, Phys. Rev. B **45**, 13749 (1992).

29. F. J. Himpsel and D. E. Eastman, J. Vac. Sci. Technol. **16**, 1297 (1979).

30. L. S. O. Johansson, R.I.G. Uhrberg, P. Martensson and G.V. Hansson, Phys. Rev. B **42**, 1305 (1990).

31. J. E. Demuth, B. N. J. Persson and A. J. Schell-Sorokin, Phys. Rev. Lett. **51**, 2214 (1983).

32. D. Haneman, Rep. Prog. Phys. **50**, 1045 (1987).

33. I. Ivanov, A. Mazur and J. Pollmann, Surf. Sci. **92**, 365 (1980).

34. E. Landemark, C. J. Karlsson, Y.-C. Chao, R. I. G. Uhrberg, Phys. Rev. Lett. **69**, 1588 (1992)

Chapter 3

Electronic Structure of Overlayer/Diamond Interfaces

Abstract

Diamond is an important semiconductor which has great potential in high temperature, high power device applications. In the fabrication process of diamond electronic devices, doping of diamond and understanding of diamond/metal interfaces are important. As a Column III element, boron is a possible p-type dopant for diamond. On the other hand, antimony is a possible n-type dopant as a Column V element. Early work reported that B and Sb are two of three cases that have positive results for incorporation into diamond by ion implantation [1]. Furthermore, boron-doped CVD diamonds have been grown in several laboratories. In addition, B and Sb play an important role in Si and Ge heteroepitaxial growth. On the Si(100) surface, epitaxial growth of Si and Ge layers has been achieved on top of the B/Si(100)-(2×1) surface at relatively low temperatures. While on the Si or Ge surface one ordered monolayer of Sb occupies the epitaxial sites and saturates the surface dangling bonds, which leads to uniform epitaxial growth. Although diamond has the same crystal structure as both silicon and germanium, it has a drastically smaller lattice and much stronger bond. This makes it very difficult to extrapolate the behaviors of boron and antimony on diamond from its behavior on either silicon or germanium. In this work, we have studied the electronic and geometric structure of B and Sb on diamond surfaces using photoelectron spectroscopy and low energy electron diffraction. Unlike

on silicon, we find that no ordered layer of boron forms on diamond, and that boron behaves differently on the C(100) surface as compared to the C(111) surface although the exact adsorption sites could not be determined. We find that boron diffuses into the substrate after high temperature annealing. Moreover, we also find that antimony strongly bonds to the diamond surface, and that antimony behaves very differently on the C(100) surface as compared to the C(111) surface. Further, we also find that the Sb/diamond system does not behave like antimony on either silicon or germanium. We attribute these results to the drastically smaller diamond lattice and the stronger C-C bond.

3.1 Introduction

I have discussed the electronic structure of the natural diamond (100) surface in the last chapter. In this Chapter, I will discuss the results of our photoemission studies of overlayer/diamond interfaces. As one of the most remarkable substances, pure diamond has great potential for many practical applications, but we have to know how to dope diamond and how to make metal contacts with diamond in order to actualize the most electronic device applications of diamond.

Diamond is one of the ideal semiconducting materials as indicated by various figures of merit (See Chapter 1). Anticipated applications include refractory devices, high-frequency devices, high-temperature devices, high-power devices and blue emitting devices. These device applications require understanding of diamond-doping, diamond-metal interfaces, Schottky and ohmic metal contacts with diamond, and band offsets at semiconducting junctions.

Diamond is essentially insulating but can be made conductive by doping with Column III or Column V elements. It is not hard to make conductive diamond either by high pressure synthesis or by the CVD process. P-type semiconducting diamond by boron doping has been carried out. Vavilov, *et al.* reported that boron and antimony have been successfully incorporated into diamond by ion implantaion [1]. However, this process introduces surface defects during implantation and the subsequent annealing process. On the field of doping diamond films, Geis, et al. [2] reported fabricating homoepitaxial semiconducting diamond using a small piece of boron placed near the diamond substrate as a source of the boron dopant. In addition, Okano,

et al. fabricated boron-doped diamond films, and used a saturated solution of B_2O_3 powder in methyl alcohol thinned by acetone as a reacting mixture [3]. Later, Ramesham *et al.* successfully synthesized boron-doped diamond films using a solid glassy matrix of B_2O_3. This oxide is quite conventionally and routinely used, and this method eliminates the problem of choosing a suitable organic solvent and use of poisonous gases. In order to confirm the nature of boron doping, Mort et al. did a infrared absorption study, in conjunction with the results on the electrical conductivity and its temperature dependence for nominally undoped and boron doped diamond thin films. They confirmed that boron doping from a gas phase precursor is substitutional in nature [4, 5].

But n-type doping of diamond has proven much more difficult. Several potential dopants were introduced into natural diamond by ion implantation, but Vavilov, *et al.* reported the only successful n-type case involved Li, which was found to be an interstitial donor with an energy level at $E_C = 0.1$ eV. However, Li-doped samples become deactived after prolonged annealing although Li is still present in the sample [6]. More recently, Okumura et al. reported n-type diamond films by the in-diffusion of lithium from the vapor phase. Although lithium incorporation was established, only small changes in electrical conductivity and no thermionic emission from donor levels were observed [7]. In the theoretic work, Kajihara *et al.* investigated the potential n-type dopants, N, P, Li, and Na, in diamond via ab initio methods. They reported that nitrogen, as a deep donor, occupies a substitutional site distorted along the (111) direction. P, Li, and Na are shallow donors, but their solubilities are very low. Therefore, these impurities need to be either incorporated by ion implantation or kinetically trapped during growth [8].

Nowadays, growth of high quality crystalline doped diamond is still rare, fundamental mechanisms involved in diamond doping, and its interfaces with other

metals are not yet well understood. On the other hand, extensive research has been done to understand the B/Si [9-11], the Sb/Si and Sb/Ge interfaces [12-14].

In the study of B/Si interfaces, it is found that boron occupies the subsurface site (S_5) on Si(111) after high temperature annealing, in dramatic contrast to other group-III metals (Al, Ga, In), all of which occupy the adatom site (T_4) (See Figure 3-1), although all those metals on Si(111) can form ($\sqrt{3}x\sqrt{3}$) reconstruction. Headrick et al., [9] from AT&T Bell Laboratories, used synchrotron x-ray diffraction in their B/Si(111) study, while Lyo et al. [10] of IBM in Yorktown Heights and Bedrossian et al. [11] of Harvard University used scanning-tunneling microscopy in their research. Similarly, on Si(100) surface boron behaves differently than other group-III metals do. At a coverage of half monolayer, B/Si(100) exhibits a (2x1) reconstruction [15], while Al, Ga, and In show (2x2) reconstruction [16]. In the studies of the electronic structures of B/Si(111) surface, it has been found that when B occupies T_4 sites all the Si surface dangling bonds are saturated while there is no resolvable new chemically shifted Si component in the core level spectra. For B-S_5 configuration, a large chemically shifted Si component has been observed, which are contributions from both Si adatoms and the surface layer Si [17]. For the B/Si(100) system, it has been found that the boron is located on the top surface as adatom, and the surface dangling bonds are not completely saturated. Epitaxial growth of Si and Ge layers on the B/Si(100)-(2x1) has been achieved at relatively low temperature [18].

In the study of the Sb/Si and Sb/Ge interfaces, it is found that high quality epitaxial Si/Ge layers can be grown using Sb as a surfactant. This is mainly due to the unique structure of Sb/Si and Sb/Ge, where one ordered monolayer of Sb occupies the epitaxial sites on the Si or Ge surface and saturates the surface dangling bonds, which leads to uniform epitaxial overlayer. Since carbon (diamond), silicon and germanium are all Column IV element, it is interesting to compare the Sb's behaviors on these

interfaces. While diamond is also a Column IV element and has the same crystal structure as silicon and germanium, its lattice is significantly smaller than that of both silicon and germanium, and its C-C bond is much stronger than the Si-Si and Ge-Ge bond. The covalent radius of antimony is 1.45 Å, only 0.09 Å shorter than the C-C bond in diamond, which is only 1.54 Å. The question arises whether antimony is going to bond to the diamond? If so, what is the overlayer geometry?

The objective of my B/C study is to find out : How does the presence of the adsorbate modify the geometric structure of the diamond surfaces? How does the adsorbate affect the electronic structure of the diamond surfaces? Is it possible to correlate the changes in electronic and geometric structure? The objective of this photoemission study of Sb/C interfaces is to improve the understanding of Sb's behavior in diamond and diamond/metal interfaces, moreover to investigate the effect of substrate lattice size on overlayer geometric structure.

3.2 Experimental

The photoemission spectra were obtained on beamline 3-1, a grasshopper monochromator, at Stanford Synchrotron Radiation Laboratory. Beamline 3-1, the New Grasshopper, is equipped with two interchangeable gratings, one of 600 lines per millimeter and the other of 1200 lines per millimeter. These two gratings allow the monochromator to deliver photons with energies from as low as 25 eV to about 1 KeV. The resolution is selected by means of adjustable entrance and exit slits. The overall instumental resolution (monochromator plus spectrometer) for this study was between 200meV to 250meV.

The experimental ultrahigh vacuum chamber (base pressure better than $7x10^{-11}$ Torr) consists of a main chamber housing low energy electron diffraction (LEED) optics, a load lock system, and a double-pass cylindrical mirror analyzer (CMA), the axis of which lies along the polarization vector of the synchrotron radiation. The sample manipulator has an on-axis configuration which allows the sample normal to be rotated in the plane formed by the CMA axis and the direction of light propagation. It is also equipped with a e-beam heater that was used to anneal the Sb/C(100) and Sb/C(111) samples.

The nature diamond surfaces to be studied were mechanically polished on a rotating wheel of cast iron periodically replenished with a mixture of diamond grit and olive oil. During polishing the grit itself is eroded. The grit size at the end of polishing is thought to be well below 1μm [20, 21]. The olive oil acts as a hydrogen source for the diamond surfaces during polishing. The diamond surface, as polished, is terminated by hydrogen atoms. All samples were outgassed at 500°C until the chamber pressure recovered to the mid tens. The reconstructed surface were obtained by e-beam heating. The diamond(100) sample was heated to 1100°C and the diamond (111) sample was annealed at 1000°C for 10 minutes. A 2x1 LEED pattern was obtained. Although diamond has a band gap of 5.5 eV, a previous study [21] found that sample charging was not a problem during our photoemission study as long as the edge of the sample surface has a good contact to the ground. The temperatures stated in this paper have an error limit of ±20°C, since the thermal couple was placed on the sample holder instead of sample surface in order to keep the surface undisturbed.

The B/diamond surface was prepared through evaporating solid B_2O_3 mounted on a tungsten filament, while reconstructed diamonds were held at ~500°C during deposition. The amount of the deposited materials was determined by the evaporation rate calibrated from an *in situ* crystal thickness monitor. These surfaces were then

annealed at several temperatures, up to 1100°C. The presence of oxygen contamination was checked with PES by monitoring the O 1s core level. The amount of O was below the detection limit. The surface geometric structure was characterized by an in situ LEED optics. Only weak intensity change of the LEED pattern was observed through the annealing process.

The Sb/diamond interfaces were prepared by evaporating antimony from a thoroughly degassed tungsten coil. Because there is no information on the antimony-diamond system, and antimony's behavior on the C(100) surface was unknown, we only deposited approximately one monolayer of antimony on the diamond samples and spectra were collected at several annealing temperatures, up to 1100°C. The surface geometric structure was characterized by an in situ LEED optics. Similar to the B/C system, only week intensity change of the LEED pattern was observed through the annealing process.

3.3 Results and Discussion

3.3.1 The B/C interfaces

The B 1s core level spectrum provides information about the chemical state of the boron. Figure 3-2 shows two B 1s core level spectra obtained from the B/C(100) sample with 210 eV photons. The top spectrum is the B 1s when B_2O_3 was deposited on the C(100) surface held at 500°C, the bottom one was taken after 1000°C annealing. For the B/C(100), there is no drastic line shape change of the B 1s core level spectra through the annealing process. On the other hand, the B 1s core level spectra show line shape change at B/C(111) interface through the deposition and annealing process. As shown in Figure 3-3, the B 1s peak had two components as deposited. That is because boron atoms are partially bound to oxygen atoms and the

C(111) surface was covered by a disordered layer. After annealing the B/C(111) sample at 1000°C, the component of B 1s at lower kinetic energy side disappears. Meanwhile, the PES spectra show that the interface is free of oxygen. These indicate that the coverage of the boron atom is much more uniform after the annealing, and that the 1000°C post annealing desorbs oxygen from the system, and that the electronic environment of the boron atoms is similar to that of each other. Moreover, the peak position of the B 1s core level obtained from the B/C(100) sample is at kinetic energy of 15.9 eV, while for the B/C(111) as deposited the B 1s core level has two components at 16.2 eV and 17.4 eV respectively. After 1000°C annealing, the B 1s located at 17.4 eV. This suggests that boron may bonds differently on the C(100) surface than on the C(111) surface. On the other hand, it is not surprising to see this more than 1 eV shift, because it has been found that the B 1s core level shows more than 5 eV shifts from the previous PES study of the B 1s core level peak [17-19]. Further, the previous study of B/Si interfaces [17, 18] has also been found that the substrate Si 2p core level PES spectra show tremendous line shape change through the boron deposition and annealing process. Thus it is interesting to ask whether the C 1s core level spectra, obtained from the B/C(100) and B/C(111) interfaces, are changed.

Figure 3-4 presents two C 1s core level spectra from the B/C(100) sample with 340 eV photon. One spectrum was taken right after the boron deposition, another one was taken after 1000°C annealing. The main change of the C 1s peak is that the peak intensity decreased after annealing. This intensity decrease is caused by the uniform coverage of the boron atom after high temperature annealing, which coincide with the information we have obtained from the B 1s PES spectra. The similar intensity reduction of the C 1s core level spectra was observed for the B/C(111) sample after annealing at 1000°C (See Figure 3-5). The line shape of the C 1s spectra for both of the (111) and (100) surfaces do not show any characteristic change. Similarly, the valence band spectra of the B/C(100) and B/C(111) samples obtained through the

process do not indicate any pronounced change (Figure 3-6 and 3-7). However, it should be noted that the valence band spectrum, obtained from the B/C(100) after 1000°C annealing (Figure 3-6), has a small extra shoulder near Fermi edge (E_k = 35.8 eV). This shoulder could originate from the platinum foil that holds diamond on the sample holder. This experimental error is causes by the small portion of the photon beam hits the metal foil, the cross section of which is much higher than semiconductor at this energy range. The re-examinations of the diamond samples with partial beam on the platinum also show that this shoulder could originate from the platinum foil. (I do not include the C 1s and B 1s CFS spectra from both B/C(100) and B/C(111) samples, because the results of C 1s CFS are indistinguishable from that of the clean diamond sample and the B 1s CFS do not display any perceptible change through the whole process). From this I deduce that boron behaves quite differently on the diamond surfaces than on the corresponding silicon surfaces. Boron does not form ordered layer on top of the diamond surfaces or beneath the diamond surfaces.

Then, Figure 3-8 displays two C 1s core level spectra from the B/C(111) sample. One spectrum was taken right after 1000°C annealing, another one was taken after 1100°C annealing. It is quite clear that the intensity of the spectrum recorded after 1100°C has increased significantly. At same time, the B 1s core level spectrum has decreased very sharply. Figure 3-9 reveals that very little amount of B is detected and a large shift of the B 1s peak towards the lower binding energy is observed. These results indicate that the boron atoms diffuse into the substrate, and incorporated with the substrate carbon atoms.

Meanwhile, a diffuse (1×1) LEED pattern with slightly streaky and fuzzy spots has been observed for the B/C(111) through the whole deposition and annealing process. Similarly, for the B/C(100) a diffuse (1×1) pattern with a high background intensity has been observed in LEED, sometimes coexisting with a diffuse (2×1) pattern. Large and diffuse spots in the LEED pattern indicate that the ordered domains

are small and a diffuse background shows that a large part of the surface is disordered. The LEED pattern could also indicate that the surface is rough.

3.3.2 The Sb/C interfaces

Figure 3-10 presents a series of normalized C 1s core level spectra from the Sb/C(100) sample taken before and after the deposition of antimony as well as after anneals at a photon energy of 340 eV. The bottom curve, labeled C:H, is the spectrum obtained from the hydrogen-terminated surface. The next one, labeled clean, is the spectrum collected from the reconstructed C(100)-(2x1) surface. The curve, labeled as deposited, is the C 1s peak obtained after the deposition of approximately one monolayer of boron on the C(100). The top five curves are the spectra collected from the Sb/C(100) sample after annealing at different temperatures. For the clean C(100) surface, deconvolution of the C 1s peak shows that the C 1s peak shifts to a lower kinetic energy relatively to that of the hydrogen-terminated (C:H) surface and a shoulder shows up at higher kinetic energy. The 0.3 eV shift is due to band bending and the broadening is due to a chemical shift attributed to the C atoms participating in the reconstruction. From the deposition of antimony through different temperature annealing, the C 1s peak broadens and shifts to lower kinetic energy. At a temperature of 550°C, the peak reverts to the line shape characteristic of the reconstructed clean surface. Figure 3-11 shows the valence band spectra of the Sb/C(100) obtained with 40 eV photons. The surface state that is 2.5 eV below the Fermi level is present in the valence band spectra since the reconstruction. There is no significant line shape change of the valence band spectra, like the C 1s peak, through the whole deposition and annealing process. Similarly, the valence band and C 1s core level spectra of Sb/C(111) sample obtained through the Sb deposition and annealing process do not indicate any characteristic change. The LEED patterns observed through the whole

process are similar to the clean surface for both the C(100) and C(111) surface. By analysis of the C 1s core level, valence band spectra and the LEED pattern only, we are not able to determine how Sb bonds to diamond surfaces. We will now turn to the examination of the Sb 4d PES spectra in the next paragraph.

Figure 3-12 shows the evolution of the Sb 4d core level on the Sb/C(100) system after approximate one monolayer coverage of boron and annealing up to 800°C. First, I would like to point out that we observe the Sb 4d peak after the 800°C anneal, with trace amounts of antimony remaining after annealing the sample as high as 1100°C. All antimony desorbs from both Si and Ge at 600°C. Since there is a large body of experimental data that confirms the covalent nature of both the Sb-Si and Sb-Ge bonds, and the desorption temperature of antimony from diamond is so high, we infer that the Sb atoms do bond to the diamond surface, and that these bonds are in fact, stronger than either Sb-Ge or Sb-Si bonds. Second, there is a reduction of the peak intensity through the annealing process. we interpret the reduction as reflecting decrease of the amount of antimony on the surface. Third, the Sb 4d peak from Sb/C(100) system broadens slightly and shifts to a lower kinetic energy as the annealing temperature increases. This broadening and shift means that the change of the chemical state of antimony, which reflects the change of antimony's bond in the Sb diffusion from surface to the substrate. As can be seen in Figure 3-13, Sb 4d peak was also detected after 800°C annealing on the Sb/C(111) sample. We conclude that the antimony atoms bond to C(111) surface by the same argument used above. Unlike the (100) system, Sb 4d core level spectra on the Sb/C(111) surface, shown in Figure 3-13, exhibit more complex line shape changes. Thus Sb acts differently on the diamond (100) surface and diamond (111) surface. After the initial light anneal, a second peak starts to grow shifted 0.8 eV towards lower kinetic energy, which indicate the Sb atoms occupy at least two different sites on C(111) surface. It is interesting to point out that the energy position of the second component is almost the same as that of the

Sb 4d peak on the Sb/C(100). But the valence band spectra on the Sb/C(111) surface exhibit little characteristic change as shown in Figure 3-14. In addition, the LEED patterns observed from 550°C to 800°C annealing were not changed, it is difficult to deduce the specific geometry from the energy shifts and number of peaks that contribute to the core level photoemission spectrum. At higher temperatures, both peaks decrease in amplitude, which we interpret as the desorption of antimony that occurs at the temperature above 1000°C.

Comparing to the Sb-Si and Sb-Ge systems, Sb behaves quite differently on the diamond surfaces. It has been shown that the Sb atoms plays a similar role on the Si and Ge surfaces. The Sb atoms adsorb in a unique environment on the surfaces. The Sb atoms eliminate the surface components of the Si 2p (Ge 3d) core level spectra by forming dimers on Si(100) (Ge(100)) surface, and trimers on the Si(111) surface [23, 24]. Due to one ordered monolayer of Sb that occupies the epitaxial sites on the Si or Ge surface that completely saturate the surface dangling bonds of the substrate, it is found that high quality epitaxial Si/Ge layers can be grown using Sb as a surfactant. It is also found that the Sb-Sb bond on Si or Ge surfaces is covalent, and the bond lengths being given by the sum of the covalent radius of the two atoms. Although silicon, germanium and diamond have the same crystal structure, the diamond lattice is significantly smaller. For instance, the diamond lattice is 17% smaller than that of silicon, it is apparent that the Sb dimers do not fit on the diamond(100) surface. In fact, it is difficult to find any adsorption sites in which an antimony atom can bond to the topmost carbon atoms and still allow the topmost carbon atoms to retain their tetrahedral coordination without significant strain in the Sb-C bonds. As can be seen from the Sb 4d spectra (Figure 3-15 [24]), the Sb 4d peak of the Sb/C(100) is much broader than that of Sb/Si(100) after annealing.

The desorption temperature for the Sb atoms on the diamond surfaces is much higher than that for both silicon and germanium indicate that the Sb-C bond is stronger than both the Sb-Si and Sb-Ge bonds.

3.4 Conclusions

We have performed a photoelectron spectroscopy and LEED study of boron and antimony on diamond (100) and (111) surfaces. Our experimental results show that the B and Sb atoms bond to the both C(100) and C(111) surfaces, and boron diffuses into substrate after annealing at 1100°C. The experimental results also reveal that boron and antimony behave very differently on the C(100) and C(111) surfaces. For antimony, upon deposition, only a one-component Sb core level is observed on both (100) and (111) samples. Upon annealing, the Sb 4d peak on the Sb/C(100) broadens slightly and shifts to lower kinetic energy. However, a second component appears in the Sb 4d spectra of the Sb/C(111) sample. For both C(100) and C(111) surface, the LEED patterns observed from deposition of one monolayer and subsequent annealing were similar to that of clean surface.

Although diamond, silicon and germanium are in the same column of the periodic table, the B and Sb atoms act differently on the substrate of diamond than both of Si and Ge substrates. We attribute these results to the drastically smaller diamond lattice and the much stronger C-C bond. We also found that the desorption of Sb on diamond occurs at the temperature above 1000°C, which indicates the Sb-C bond is the strongest one among Sb-C, Sb-Si and Sb-Ge bonds.

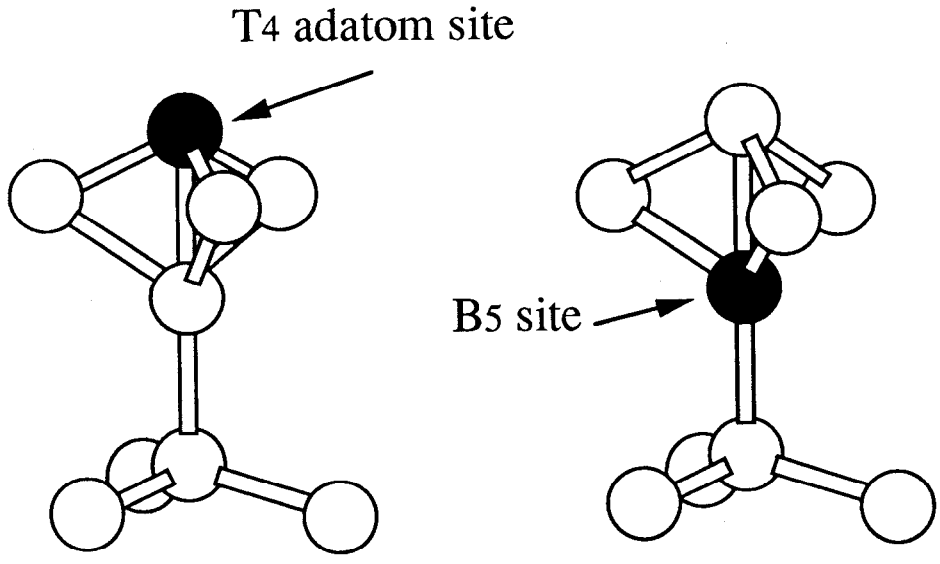

Figure 3-1 Illustration of T4, adatom site, and B5, the site underneath the adatom.

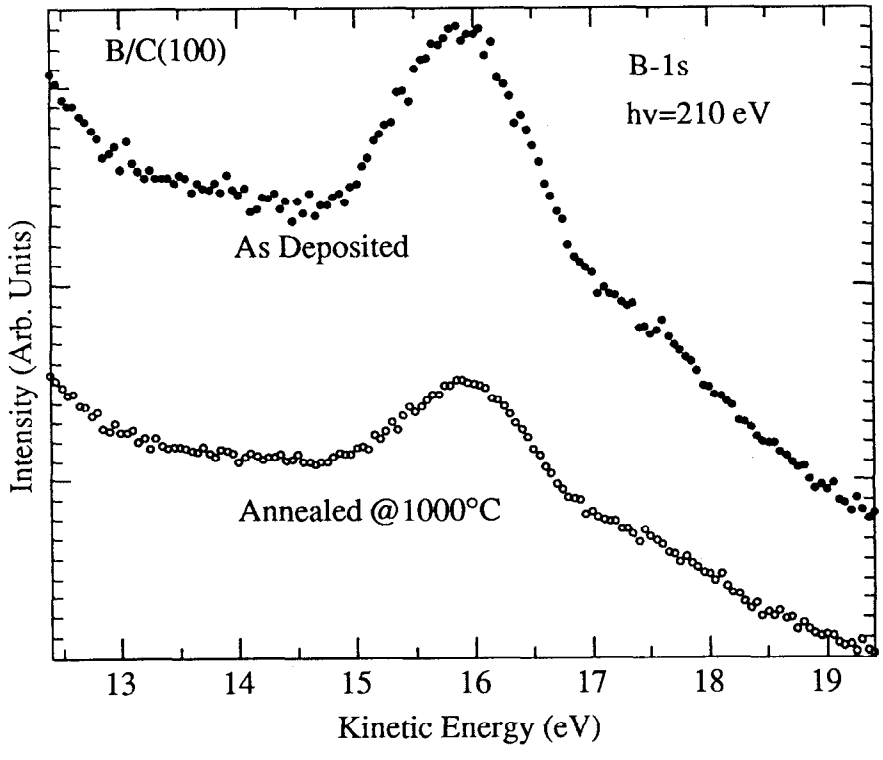

Figure 3-2 PES B 1s core level spectra (hν = 210 eV) at the 1ML B/C(100) interface.

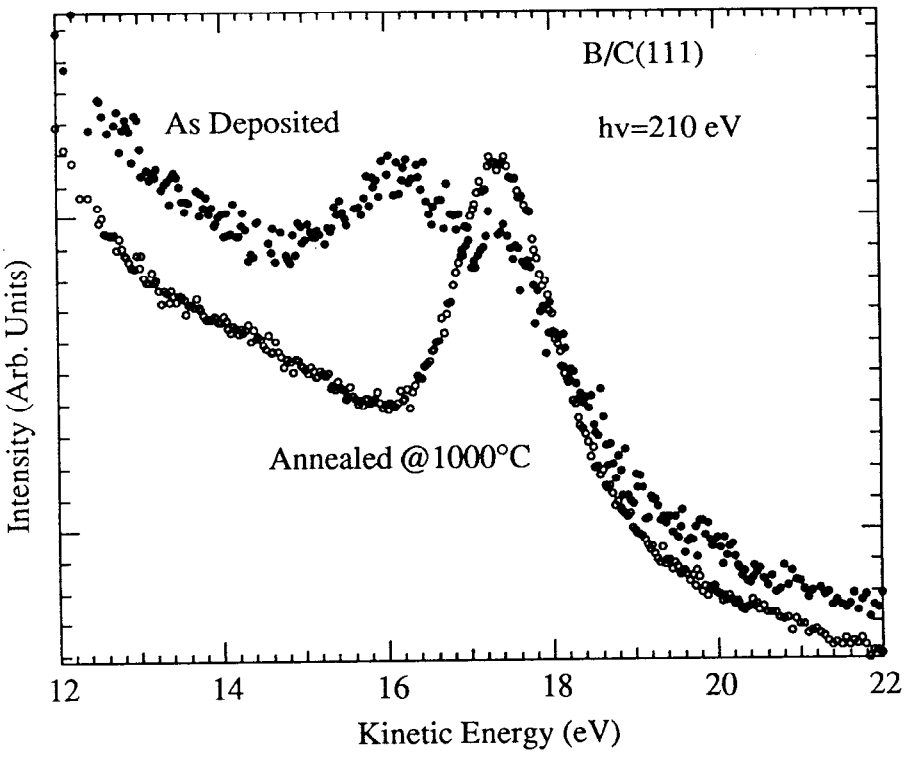

Figure 3-3 PES B 1s core level spectra (hν = 210 eV) at the 1ML B/C(111) interface.

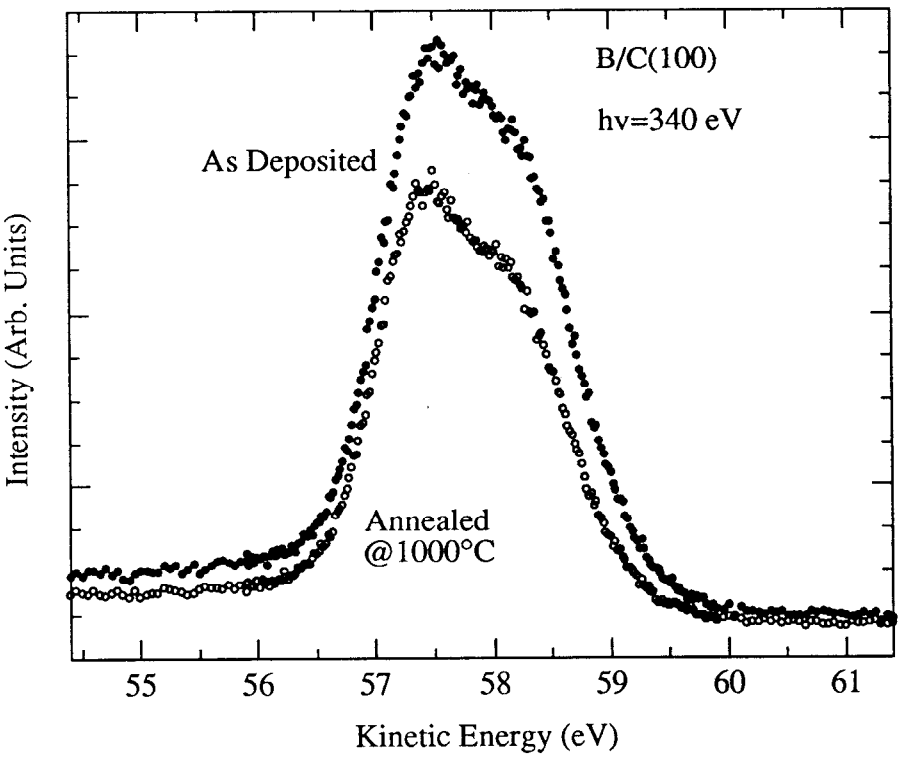

Figure 3-4 The C 1s core level spectra, taken at hν = 340 eV, of the B/C(100) system.

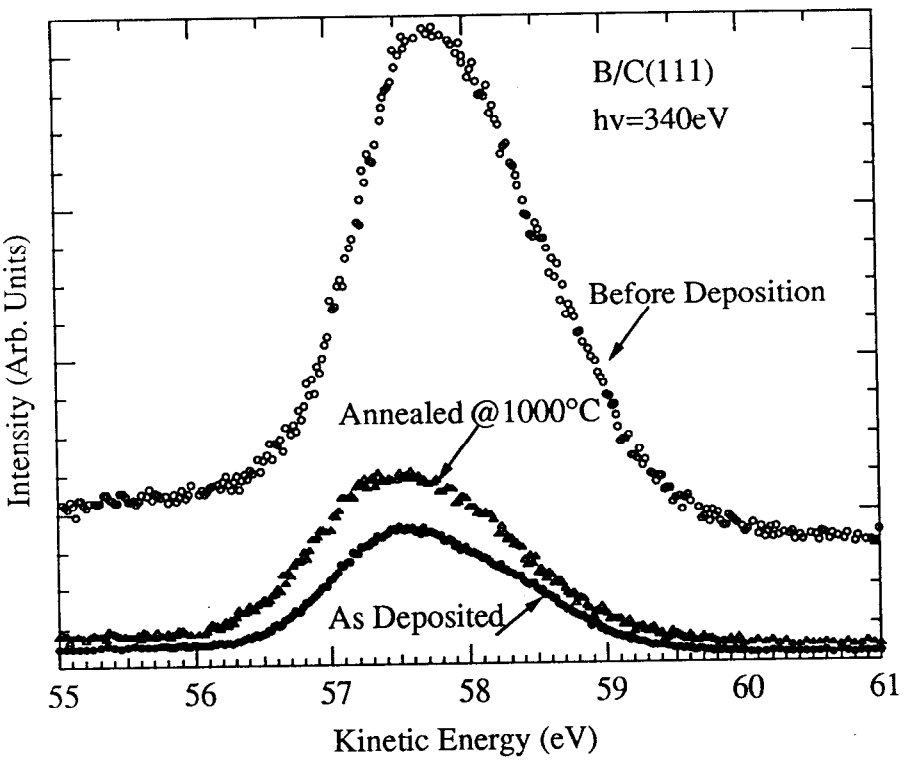

Figure 3-5 The C 1s core level spectra, taken at hν = 340 eV, of the B/C(111) system.

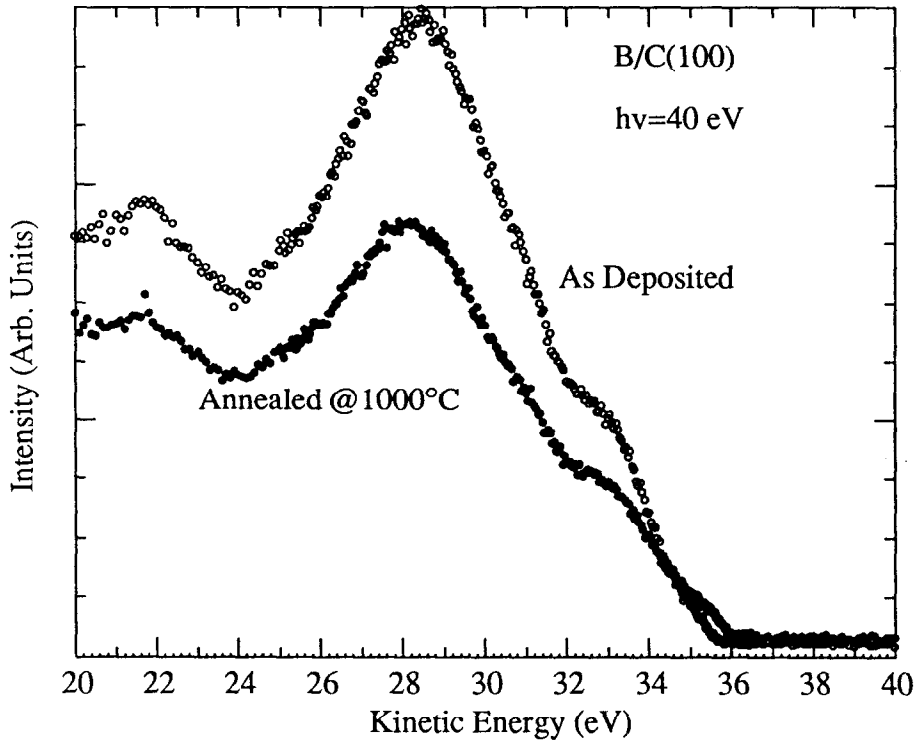

Figure 3-6 The valence band spectra of the B/C(100) obtained with 40 eV photons.

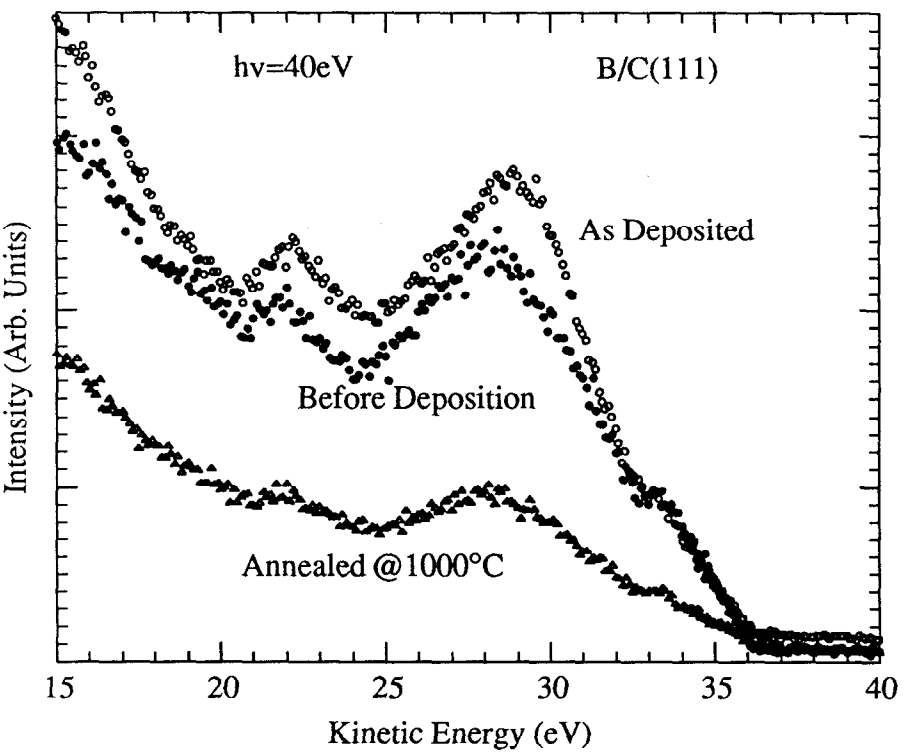

Figure 3-7 The valence band spectra of the B/C(111) obtained with 40 eV photons.

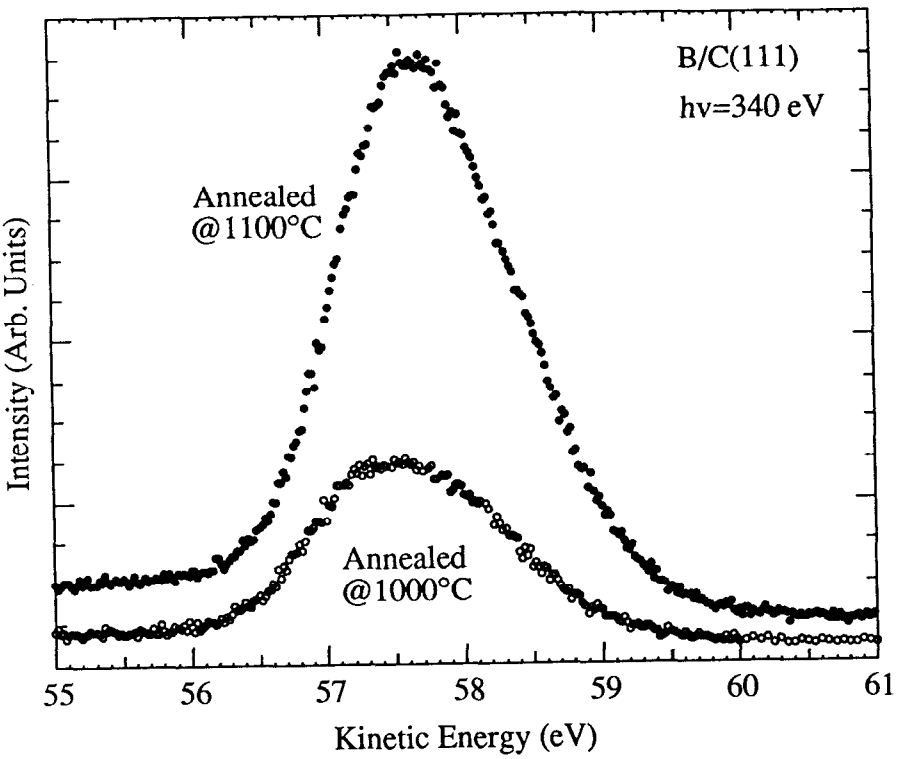

Figure 3-8 The C 1s core level spectra, taken at hν = 340 eV, from the B/C(111) surface annealed at 1000°C and 1100°C respectively.

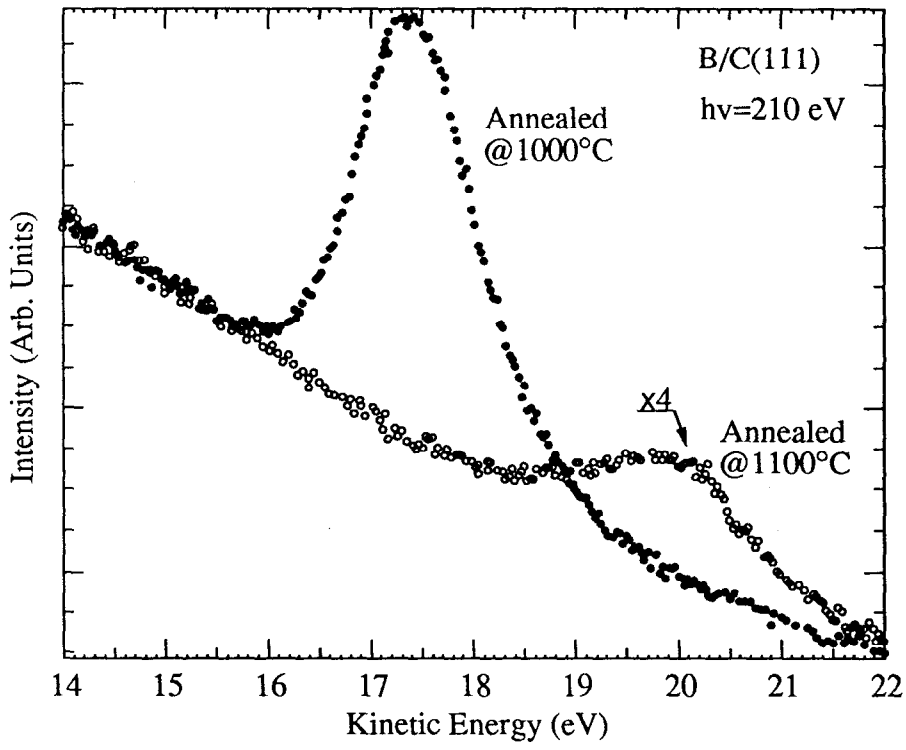

Figure 3-9 The B 1s core level spectra, taken at hν = 210 eV, from the B/C(111) surface annealed at 1000°C and 1100°C respectively.

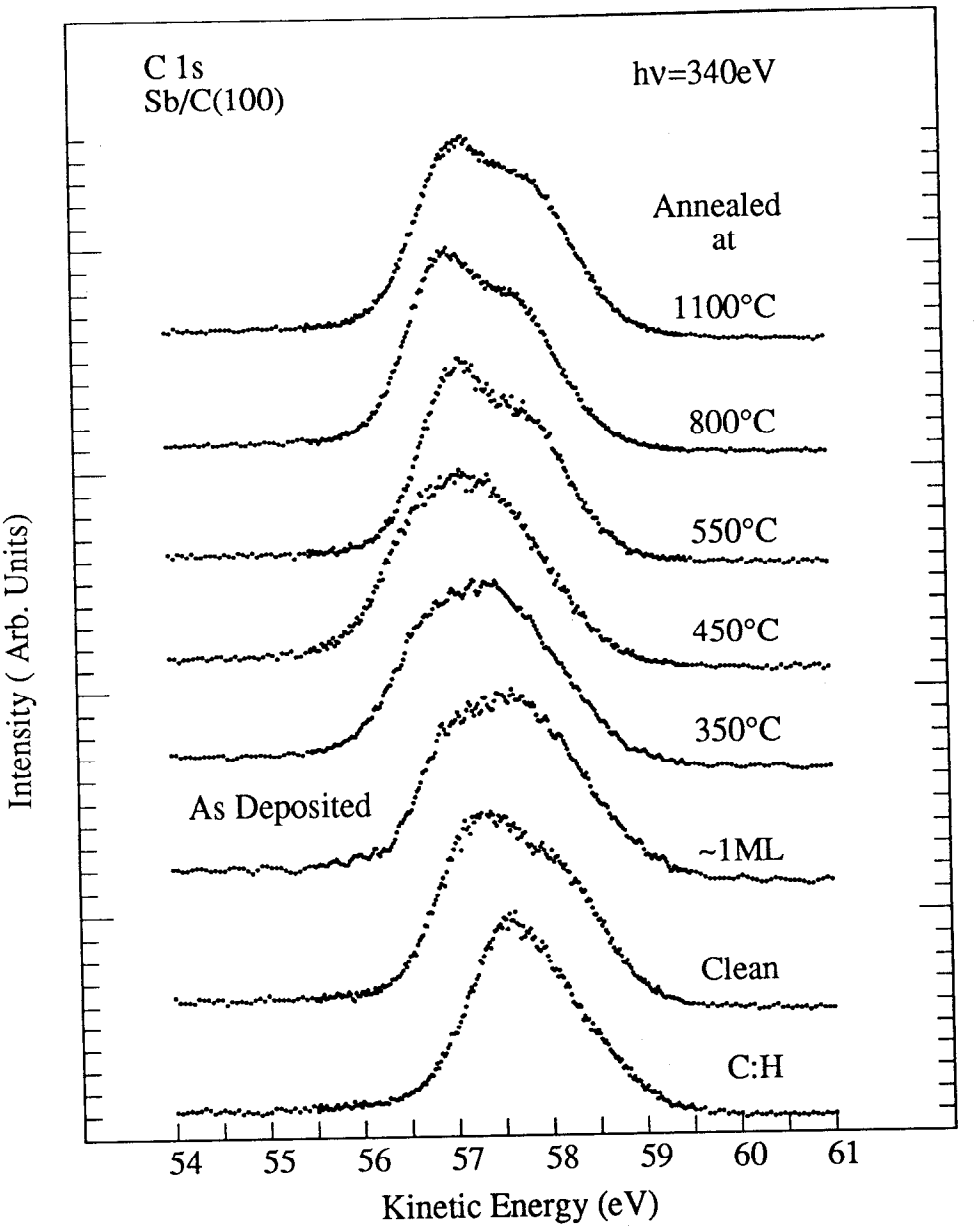

Figure 3-10 A stack of the C 1s core level spectra from the Sb/C(100) system taken at a photon energy of 340 eV.

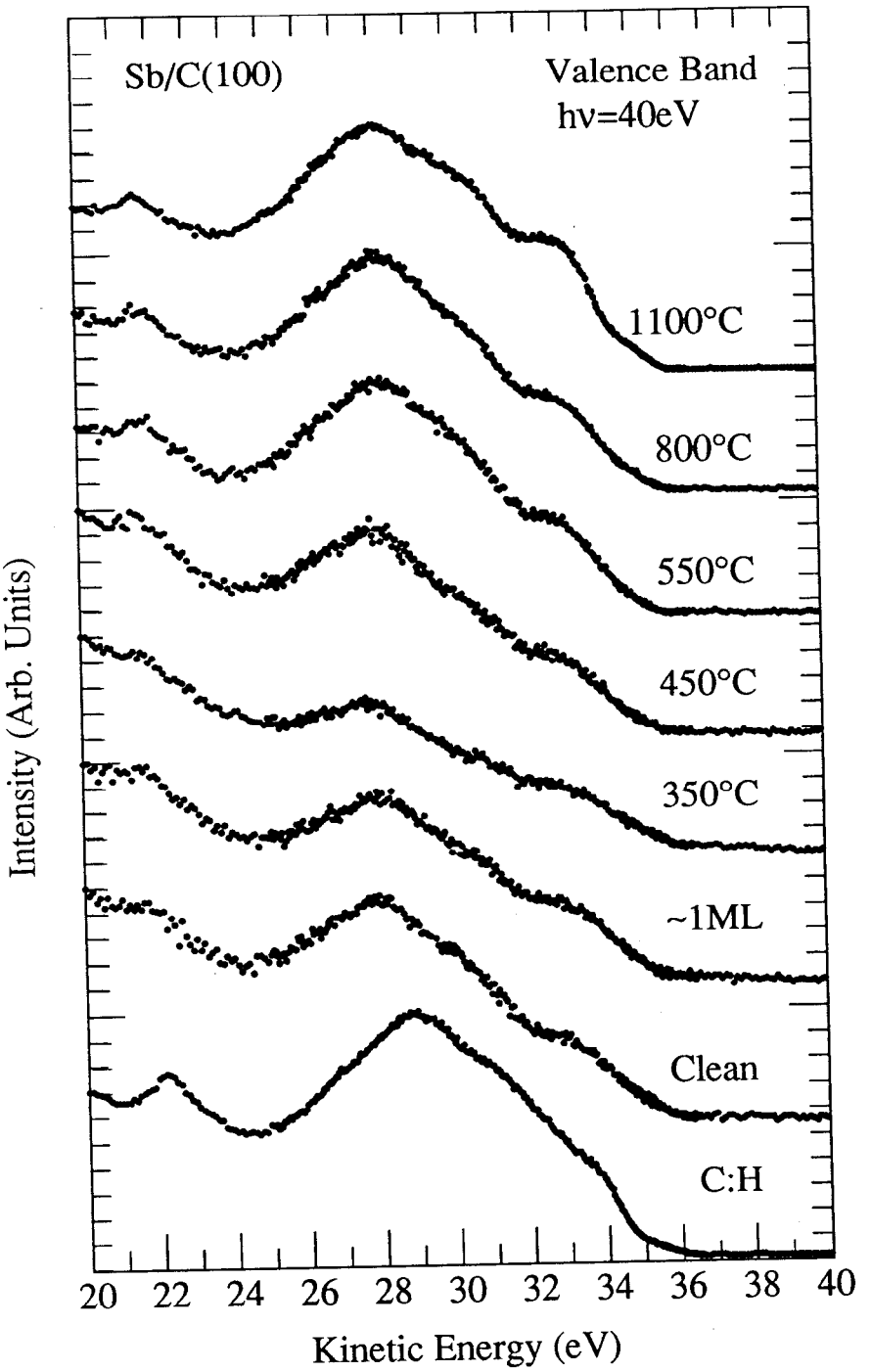

Figure 3-11 The valence band spectra of the Sb/C(100) obtained with 40 eV photons.

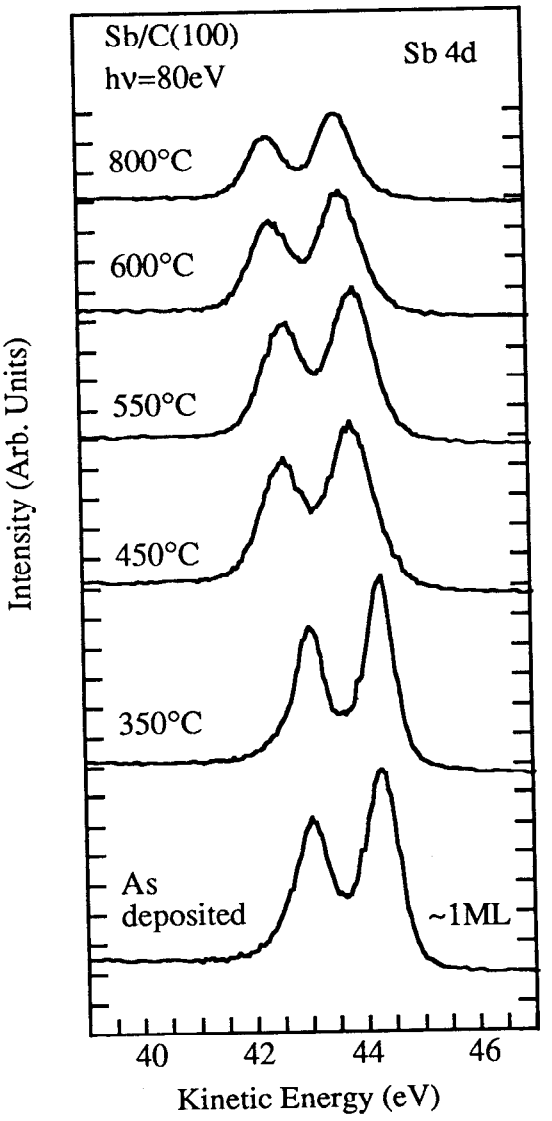

Figure 3-12 The evolution of the Sb 4d core level on the Sb/C(100) system.

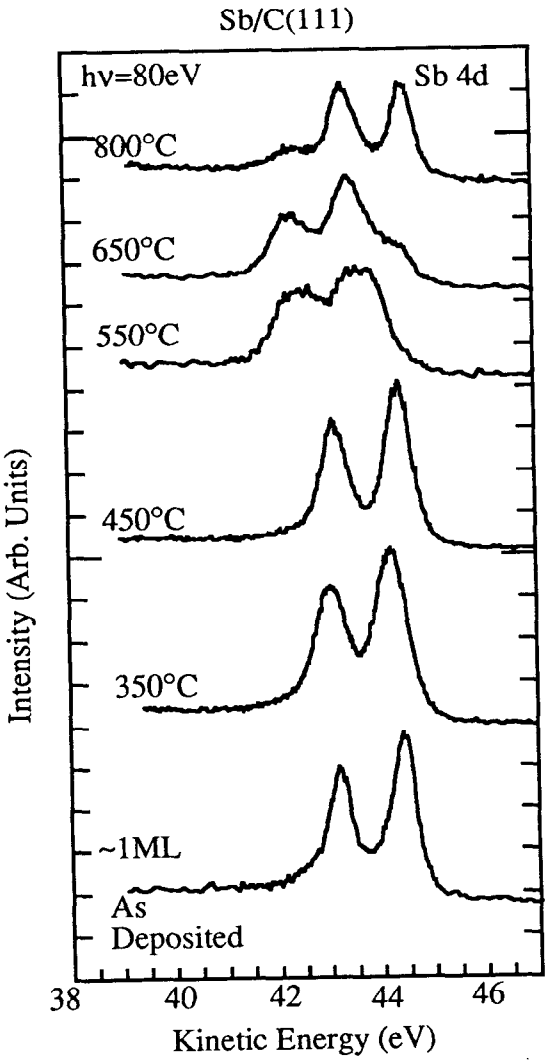

Figure 3-13 The evolution of the Sb 4d core level on the Sb/C(111) system.

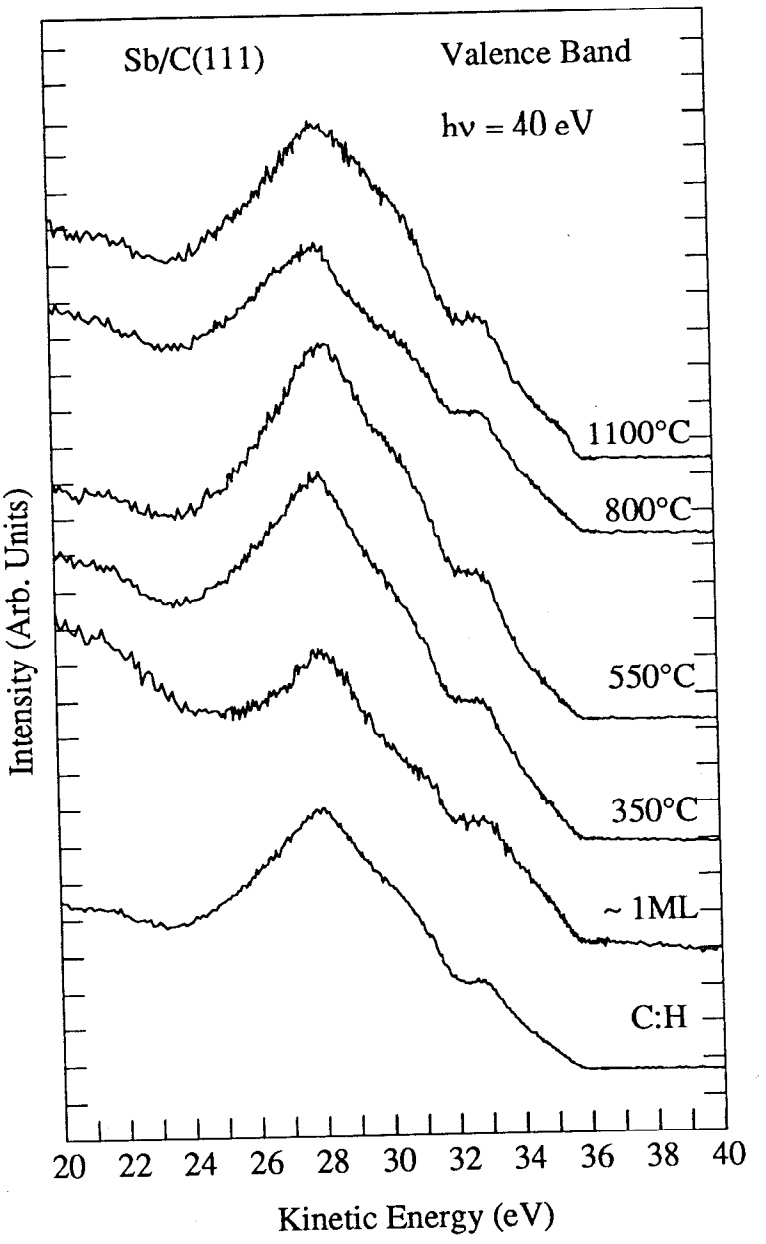

Figure 3-14 The valence band spectra of the Sb/C(111) obtained with 40 eV photons.

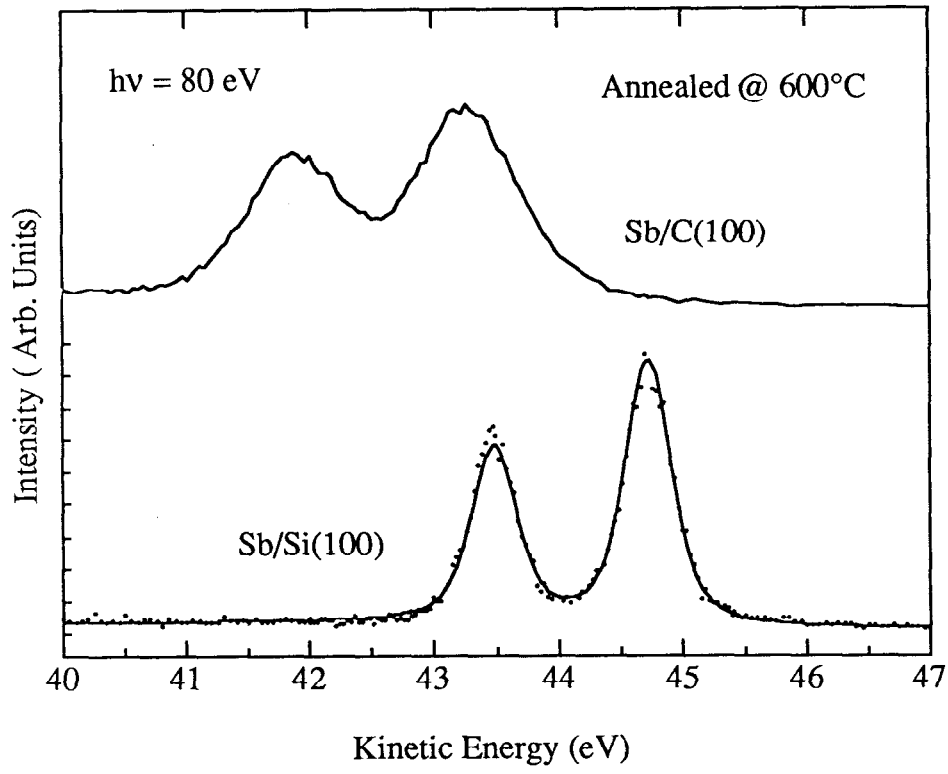

Figure 3-15 The Sb 4d spectra on the Sb/Si(100) [23] and Sb/C(100) system obtained with 80 eV photons.

References:

1. V.S. Vavilov, E. A. Konorova, E. B. Stepanova, and E. M. Trukhan, Sov. Phys. Semicond. **13**, 635 (1979).

2. M. W. Geis, D. D. Rothman, J. J. Zayhowski, D. C. Smythe, D. K. Smith, and G. A. Ditmer, diamond and Diamond-like Materials Synthesis, G. H. Johnson, A. R. Badzian, and M. W. Geis (Editors), Materials Research Society, p. 115 (1988).

3. K. Okano, H. Naruki, Y. Akiba, T. Kurosu, M. Iida and Y. Hirose, Jap. J. of Appl. Phys. **27**, No. 2, L173, (1988).

4. J. Mort, M. A. Machonkin, and K. Okumura, Appl. Phys. Lett. **58** 1908 (1991).

5. J. Mort, K. Okumura, and M. A. Machonkin, Philos. Mag. **63** 1031 (1991).

6. V. S. Vavilov, Radiat. Eff. **37**, 229 (1978).

7. K. Okumura, J. Mort, and M. Machonkin, Appl. Phys. Lett. **57**, 1907 (1990).

8. S. A. Kajihara, A. Antonelli, and J. Bernholc, Phys. Rev. Lett. **66** 2010 (1991).

9. R. L. Headrick, I. K. Robinson, E. Vlieg, and L. C. Feldman, Phys. Rev. Lett. **63**, 1253 (1989).

10. I.-W. Lyo, E. Kaxiras, and Ph. Avouris, Phys. Rev. Lett. **63**, 1261 (1989).

11. P. Bedrossian, R. D. Meade, K. Mortensen, D. M. Chen, J. A. Golovchenko, and D. Vanderbilt, Phys. Rev. Lett. **63**, 1257 (1989).

12. R. Cao, X. Yang, J. Terry, and P. Pianetta, Phys. Rev. B **45**, 13749 (1992).

13. M. Richter, J. C. Woicik, J. Nogami, P. Pianetta, K. E. Miyano, A. A. Baski, T. Kendelewicz, C.E. Bouldin, W. E. Spicer, C. F. Quate, and I. Lindau, Phys. Rew. Lett. **65,** 3417 (1990).

14. D. H. Rich, F. M. Leibsle, A. Samsavar, E. S. Hirschhorn, T. Miller, and T.-C. Chiang, Phys. Rev. B **39**, 12758 (1989).

15. R. L. Headrick, B. E. Weir, A. F. J. Levi, D. J. Eaglesham, and L. C. Feldman, Appl. Phys. Lett. 57, 2779 (1990)

16. A. A. Baski, J. Nogami, and C. F. Quate, J. Vac. Sci. Technol. A 8, 245 (1990)

17. R. Cao, X. Yang, and P. Pianetta, SLAC-PUB-6076, presented at the 39th AVS National Symposium, Chicago, IL, November, 1992.

18. R. Cao, X. Yang, and P. Pianetta, J. Vac. Sci. Technol. B, **11**, 1455 (1993).

19. M. W. Ruckman, M. F. Murray, J. K. Mowlem and D. R. Strongin, J. Vac. Sci. Technol. A, **11**, 2477 (1993).

20. E. Bruton, Diamonds (NAG Press, London, 1970).

21. Grodzinski, Diamond Technology (NAG Press, London, 1953).

22. B. B. Pate, Surf. Sci. **165**, 83 (1986).

23. M. Richter, Ph.D. Thesis, Department of Applied Physics, Stanford University, 1993.

24. J. C. Woicik, T. Kendelewicz, K. E. Miyano, P. L. Cowan, C. E. Bouldin, B. A. Karlin, P. Pianetta, W. E. Spicer, Phys. Rev. B **44**, 3475 (1991).

Chapter 4

Electronic Structure of Single Crystal C_{60}

Abstract

This chapter reports angle-resolved photoemission data from single crystals of C_{60} cleaved in UHV. Unlike the other forms of pure carbon, the valence-band spectrum of C_{60} consists of many sharp features that essentially can be accounted for by the quantum chemical calculations describing individual molecules. This suggests that the electronic structure of solid C_{60} is mainly determined by the bonding interactions within the individual molecules. In this chapter, I review an experiment in which I observed remarkable intensity modulations of the photoemission features as a function of photon energy, suggesting strong final state effects. Finally, the chapter addresses the issue of the band width of the highest occupied molecular orbital (HOMO) state of C_{60}. I assert that the width of the photoemission peak of C_{60} does not reflect the intrinsic band width because it is broadened by the non 0-0 transitions according to the Franck-Condon principle. This viewpoint provides a possible reconciliation between the photoemission data and that measured by other techniques.

4.1 Introduction

The last two chapters have discussed the electronic structure of natural diamonds. This chapter presents the results of the photoemission studies of single crystal C_{60}, a newly discovered basic form of carbon. While solid C_{60} is quite different in structure from either of the other forms, it is instructive to compare and contrast the buckyball's electronic structure with that of diamond.

The carbon atom is the most intensely studied of all the elements. For centuries we believed the element carbon existed in only two basic, allotropic, and well known forms: diamond and graphite. In hard, sparkling diamond, the carbon atoms are arranged in little pyramids, while soft, dull, slippery graphite consists of sheets of carbon atom hexagons.

Research in the United States and Europe has now confirmed the existence of the third previously unknown form — buckminsterfullerene (C_{60}) and its relatives, the fullerenes (C_{24}, C_{28}, C_{32}, C_{70}, and so on). The C_{60} molecule is referred to as buckminsterfullerene, buckyball, or C_{60}. This molecule was named after the American architect R. Buckminster Fuller, who designed a geodesic dome with the same fundamental I_h symmetry as that of the C_{60} molecule. The C_{60} molecule has a highly unusual structure, in which 60 carbon atoms are joined together as a cage consisting of 20 hexagons and 12 pentagons in the form of a soccer ball, as depicted in Figure 1. This highly symmetric structure gives C_{60} an entire range of interesting properties and promising practical applications, such as superconductivity and the ability to trap other elements. These properties are different from those of either diamond or graphite

The discovery of the C_{60} is the result of the endeavors of many dedicated scientists. Jones, Osawa, and Yoshida are among the pioneers who made hypotheses about the buckyball over twenty years ago. In 1966 Jones [1] conceived of it as a "hollow molecule" made of curled up graphite sheets. In 1970, Osawa and Yoshida [2,

3] also envisioned the "superaromaticity" which might accompany electron delocalization over a three dimensional truncated icosahedral pure carbon molecule. Almost twenty years after the existence of a spherical carbon cluster was first imagined, Kroto and Smalley *et al.* [4] identified, for the first time, fullerene C_{60} in carbon vapor produced by the laser irradiation of graphite; they also correctly conjectured about the structure of buckyball. But because the cluster chemists had only fractions of a milligram of C_{60} to work with, they were not able to confirm their prediction. It was not until five years later, in 1990, that the physicists Kräschmer, Lamb, Fostiropoulos, and Huffman [5] made a breakthrough. They discovered a way of synthesizing pure buckyball in bulk, and were thus able to verify the existence of the molecule. The discovery of the C_{60} opened up new fields of chemistry, physics, and materials science. In recognition of this milestone, *Science* Magazine named C_{60} "the molecule of the year" for 1991 [6].

The availability of macroscopic quantities of buckyball makes it possible to discover its astonishing chemical versatility, its interesting physical properties, and its promising practical applications. For example, chemists learned that C_{60} reacts with alkali metals such as potassium and rubidium, and that it absorbs dozens of these reactive chemical species; physicists found high-temperature superconductivity in alkali doped C_{60} [7-9], and observed a large non-linear optical response in C_{60} [10]. Although the buckyball's practical applications have so far been limited by cost, researchers have already found that coating a Si substrate with C_{70} increases the growth rate of a CVD grown diamond film by 10 orders of magnitude over that on untreated silicon.

These and other interesting properties of C_{60} have stimulated research activities over the past three years [11]. By now, experimenters have revealed the geometric structure [12], the transport characteristics [13], and electronic structure [14-18],

among other properties, of this novel form of carbon. In the meantime, theoreticians predict that C_{60} is a semiconductor with a direct gap of 1.5 eV [19].

By 1991 scientists had not only gained a lot of information on molecular C_{60}, but also knew how to grow single crystal C_{60}. A group at the IBM Almaden Research Center in San Jose has grown single-crystal C_{60} by sublimation from chromatographically purified C_{60}, which provided the sample for my experiment and made this chapter possible.

Science has always believed that structure illuminates function and vice versa. Let's compare the structures of the three different pure carbon solid in detail (see Figure 2). Unlike the other crystalline forms of carbon, diamond and graphite, solid C_{60} is a molecular crystal of pure carbon. The C-C bonds within an individual C_{60} molecule are 1.40 Å and 1.46 Å long. This length is significantly shorter than the smallest C-C nearest neighbor distance between the molecules, which is about 3 Å. Although the C-C bond within the C_{60} molecule is shorter than the bond in graphite (1.42 Å and 3.40 Å) and diamond (1.54 Å), it is less dense than both graphite and diamond (Figure 2 shows the contrasting crystal structures in these forms of carbon [20]). Using this information, we can construct a model of the solid C_{60} that is comprised of well-separated C_{60} molecules, each one of which consists of 60 tightly bonded carbon atoms. An understanding of C_{60}'s unique crystalline structure is essential for interpretation of its photoemission data.

This chapter presents the results of the experimental studies of C_{60} single crystals. It focuses on two primary topics which are important for the understanding of many interesting properties of the fullerenes: (i) The electronic structure of single crystal C_{60} is mainly determined by the bonding interactions within individual molecules; (ii) the band width of this material is induced by electron hopping between the C_{60} molecules. I have observed that the valence band spectrum of C_{60} exhibits many sharp features, which can be very well accounted for by the electronic states of

the individual molecule with small modifications caused by the band effects in the solid. In contrast, the spectra of graphite and diamond show features broadened by large energy dispersion. Furthermore, I have observed very strong intensity modulations of the photoemission features as a function of photon energy. This modulation in intensity is indicative of final state effects, suggesting that one should be very careful in interpreting the photoemission data of C_{60}.

The width of the conduction band is an important issue for a theoretical understanding of the mechanism of superconductivity. Because of the repulsive nature of the electrons, a narrow band does not favor the traditional electron-photon coupling mechanism. The experimental results of the band width are currently controversial. Measurements such as the infrared (IR) reflectivity, nuclear magnetic resonance (NMR), critical field, and magnetic susceptibility give band widths of about 80-200 meV [21-25]. This range of band width values was obtained indirectly from the density of states measured in these experiments. In contrast to these results, the peak widths for both the highest valence band state and the lowest conduction band state range from 800 meV to 1200 meV in the existing photoemission spectra from polycrystalline samples [14-18]. The values for the photoemission peak widths are significantly larger than the energy resolution in the experiments, which are typically of the order of 100 to 200 meV. If these values from photoemission data are taken as the band widths [16], then the photoemission results and the results obtained by other measurements differ by about an order of magnitude. I performed the first angle-resolved photoemission experiments on single crystal C_{60} to address the issue. This experiment found that although the first valence band peak has a width of about 800 meV, it disperses by as little as 50 meV, even with substantial changes of electron crystal momentum. From an analysis of my results and the gas phase data in the literature, I have concluded that the peak width that one measures from photoemission data may be dramatically modified by final state effects, and thus may not reflect the

true band width, which is substantially narrower. I further suggest that the band width of the system is much narrower than the PES peak width. This observation provides a possible reconciliation between earlier photoemission results and those obtained by other measurements.

4.2 Experimental

It is helpful to know how to make single crystal buckyball. The C_{60} molecules were produced by the carbon arc method [12], followed by toluene extraction and chromatographic separation. The resulting material was freed from the solvent by heating it at 250°C in a quartz tube at 10^{-7} torr vacuum, followed by sublimation at 450°C. From this material, small crystals, typically 50 microns in size, were sublimed in a sealed tube with a small temperature gradient. These small crystals were placed in a new tube and once again baked at 120°C for about 10 hours, while pumping the tube to keep it at an active vacuum of 10^{-7} torr. Then the tube was sealed off again and the material that resulted from the baking was used to grow larger crystals by condensation out of the vapor phase.

The structure and the quality of the single crystal were examined in different experiments. Using high-resolution transmission electron microscopy (TEM) and electron diffraction, the IBM group found that the crystals grown by this method have either fcc or hcp structures, and sometimes observed stacking faults in the crystals [26]. The transmission Laue pattern, as shown in Figure 3, verifies the high quality of the single crystal samples . The Laue pattern was obtained with the X-ray beam perpendicular to the cleaved surface plane. Transmission mode is preferable to backscattering Laue in this case, because the carbon atom has a very small backscattering amplitude and C_{60} has a very small x-ray absorption coefficient. I

typically obtain two types of diffration patterns, with clear diffraction spots in three- or six-fold symmetry, respectively. These diffraction patterns do not have any stripes, which implies that the samples are indeed high-quality single crystals. I believe that three-fold Laue pattern was taken along (111) directions of an fcc crystal, while the six-fold Laue pattern was taken along (0001) directions from an hcp crystal. Even though an fcc structure with a stacking fault may also give a six-fold pattern, but this stacking fault must be ordered. It is important to note that the Laue pattern is different from the mono-energetic, high energy electron diffraction pattern. In real space, the crystals also appear to be different, one showing triangular faces, the other hexagonal faces. I have performed angle-resolved photoemission measurements on both types of samples, and the experimental results are qualitatively the same as those I will discuss in Section 4.3.1.

The photoemission study of C_{60} was performed in a VG ADES 400 system with a hemispherical energy analyzer at the TGM beam line I-2 of the Stanford Synchrotron Radiation Laboratory. The base pressure of the main chamber during the experiment was 2×10^{-10} torr, and the overall energy resolution was about 200 meV. An irregularly shaped single crystal of C_{60} was cemented to a post, and then another post (called "top post") was cemented to the top of the sample. The samples on the holder were then introduced into the ultrahigh vacuum (UHV) chamber through a fast entrance load-lock and cleaved in situ by knocking the top post off at room temperature. The surface areas of the cleaved crystals ranged from 0.2 mm^2 to 0.3×0.4 mm^2, which were large enough for our photoemission experiment albeit with a limited counting rate. Since the C_{60} is a semiconducting material, the sample showed some charging. But charging was controlled by coating the sides of samples with a conductive material, shining low-energy electrons on the sample with a flood gun, and controlling the intensity of the synchrotron light. The data reported here were collected after the charging had stabilized.

4.3 Results & Discussion

4.3.1 Valence band spectra and comparison with that of graphite and diamond

Figure 4 shows two photoemission spectra recorded at normal emission with photon energies of 60 and 100 eV, respectively. These spectra are very similar to data taken from polycrystalline C_{60} films and C_{60} molecules in the gas phase[15-18]. The similarity of the single crystal and gas phase data indicates that the electronic structure of the molecule is retained, to a large extent, while the solid forms from the molecules. As I discuss in detail in Section 4.3.3, I find no evidence of a sizable energy dispersion. For a comparison, I have also included in Figure 4 angle-integrated spectra from graphite [27] and diamond [28]. The valence band spectra of graphite and diamond consist of broad features from dispersive bands. In contrast, the photoemission data from C_{60} crystals exhibit very distinct valence band features as marked. These valence band features actually originate from the molecular states that are not significantly modified by energy dispersion in C_{60} crystal. This point is very clear from a comparison of our experimental data with the results of a molecular cluster calculation represented by vertical bars in Figure 4 [19]. We can see that the data agree remarkably well with the cluster calculation, which indicates that the electronic structure of the C_{60} crystal is mainly determined by the molecular bonding of the individual C_{60} molecules, and that the effect of the energy dispersion is relatively small. This conclusion is also supported by the fact that photoemission spectra from the solid film and the gas phase are very similar [14]. The gas phase photoemission data are entirely determined by the bonding of individual C_{60} molecules. This result is not surprising, since according to the crystal structure as depicted in Figure 2, the bond length of two carbon atoms in adjacent molecules is almost 3 Å, that is, much longer than the atomic distance within a molecule (1.4 Å). Therefore, the intra-molecular bonding dominates the electronic structure.

The difference between the spectra of C_{60} and that of graphite and diamond can be understood from the crystal structure in Figure 4-2. The bands in graphite derive mainly from the sp^2 bonds determined by the in-plane bond length of 1.42 Å and the free-electron like π-bonds. The bands of diamond derive mainly from the sp^3 bonds with an interatomic bond length of 1.54 Å. Because of the relatively short atomic distances involved in graphite and diamond, there are large wave function overlaps and these bands are very dispersive, resulting in broad valence band features in Figure 4-4. The bonding of C_{60} is a mixture of sp^2 and sp^3 hybrids. However, the energy dispersion of C_{60} is determined by the ~ 3Å bond length in adjacent molecules. Because of this significantly larger bond length, the energy dispersion is much smaller.

4.3.2 Photon energy dependence of the valence band spectra

The discussion in Section 4.3.1 leaves us with the general picture that the electronic structure of C_{60} as measured by photoemission is mainly determined by the molecular states, with small modifications due to the formation of narrow bands in the solid. In this section, I will discuss interesting intensity modulations of photoemission spectra as a function of photon energy. This dramatic photon energy dependence of the photoemission intensity suggests the fact that the photoemission final state (or intermediate resonance state) retains much of the molecular character of C_{60}, and that the final state effects are important for an understanding of the photoemission data.

Figure 4-5 shows energy distribution curves (EDC) spectra of a C_{60} crystal taken at various photon energies. The intensity of the C_{60} valence band features modulates dramatically with the photon energy. For example, the intensity of feature 1 shows a minimum at 35 eV and a maximum at 47.5eV, but the intensity of feature 2 reaches opposite extremes at these photon energies. This photoemission intensity modulation is likely to be related to final state effects.

To further investigate the matter, I performed a more detailed study of this issue using the constant initial-state spectroscopy (CIS) technique. The CIS technique was first employed by Lapeyre et al. for a measurement of the density of final states of KCl [29]. In this type of spectroscopy, electrons from the same initial-state energy are excited to different final-state energies by a synchronous scanning of photon energy and the pass energy of the electron analyzer. Figures 4-6 and 4-7 show the CIS scan of the C_{60} crystal. These spectra were normalized by the mesh current monitoring the photon beam intensity from the monochromator. All the initial state energy (E_i) labeled in the figures is relative to the highest occupied molecular orbital. Besides the primary photoemission process, secondary processes such as electron-electron scattering contribute to the EDC spectrum. To separate the primary process from the secondary processes in the CIS data, all the spectra presented in Figure 4-7 are obtained in the following method: two CIS spectra (see Figure 4-6) were obtained from the peak (P) and the valley (V) at higher kinetic energy as indicated in Figure 4-4. The CIS-P is the spectrum excited from the initial state at the peak of the EDC spectrum, and the CIS-V is the spectrum excited from the state in the valley of the EDC spectrum that is mainly from the secondary processes. The bottom curve CIS (E_i) is obtained by subtracting the CIS-V from CIS-P to eliminate the background emission.

Figure 4-7 presents a series of CIS spectra excited from the peaks of valence band EDC curve after subtracting the background emission. The initial-state of the topmost curve is the highest occupied molecular orbital (HOMO) state, and the initial state of the second curve is the second highest occupied state. A previous study of polycrystalline thin film reported only the first two curves, and the way to normalized the data in that paper is also different from ours [30]. The authors of the earlier paper normalized the intensity of features 1 and 2 to that of feature 4. We can see that the upper three curves show strong intensity variation with photon energy, which are very

different from the carbon atomic photoionization cross section and the graphite data [27]. Furthermore, these intensity modulations of different photoemission features exhibit very clear anti-phase relations. For example, the first peak reaches a maximum at the same photon energy as the second peak reaches a minimum. The bottom three curves, excited from the deeper C_{60} valence band feature, attenuate with photon energy monotonically. Part of this lack of structure is probably due to the difficulties in subtracting the secondary electrons from these features at higher binding energies. It is clear that the CIS curve excited from peak 4 (E_i = -9.0 eV) shows intensity modulation too. This shows that the assumption in the earlier paper that this feature should exhibit no intensity modulation because of the mixed nature of π and σ bonds is only a crude approximation [30].

The interesting phase relation of the intensity modulations of the first three features is probably related tto some sort of symmetry selection rules. Because the hollow cage structure of C_{60} is very close to a sphere, the molecular orbitals may be crudely characterized by the angular momentum quantum number l. The angular part of the wave function is defined by the spherical harmonic function $Y_{lm}(\theta, \phi)$. The energy of the state is proportional to:

$$\frac{h^2}{8m\pi^2}\frac{l(l+1)}{r^2} \qquad \text{with a degeneracy of } 2l+1.$$

The states with even l have even symmetry and those with odd l have odd symmetry. The C_{60} molecule belongs to the icosahedral point group, and using group theory we can determine the allowed transitions between the states. The highest occupied molecular orbital (HOMO) of the C_{60} valence band corresponding to the l = 5 π-derived state has an odd symmetry, and the second feature corresponds to the l = 4 π-derived state, and has an even symmetry [31]. According to parity selection rules, if the transition between the peak 1 state and a final state is allowed (enhancing the

intensity of the CIS curve), then the transition between the peak 2 state and the same final state is forbidden (suppressing the intensity of the CIS curve). (note, check feature 3) While we can have a qualitative understanding of the intensity modulation from the above simple analysis, a more detailed calculation based on the above model and free-electron like final states show much more oscillation than experimental results. I thus suggest that the final states of C_{60} well above the vacuum level retain much of the molecular character, and I would like to see more sophisticated theoretical calculations that explain this interesting intensity modulation.

The remarkable intensity modulations discussed in this section, and shown in figures 4-4 to 4-7 suggest that the final state effects are very strong in C_{60}; therefore one has to be cautious in interpreting photoemission data from this system. This leads us to the issue of the band width of C_{60}. As discussed in the introduction, some earlier photoemission data were interpreted to give a band width that is an order of magnitude larger than the results of other experiments. The next section will show that the final state effects (not necessarily those which were discussed in this section, but effects of vibronic nature) actually make the interpretation of photoemission data a very complicated task and that the photoemission peak width does not simply reflect the band width as was interpreted previously [16].

4.3.3 Angle-resolved photoemission and its implication on the band width

As I indicated in the introduction, the issue of the energy band width is very important for an understanding of many properties of solid C_{60}, in particular the mechanism of superconductivity. The angle-resolved photoemission experiment has been a very powerful tool in the study of the band width of solids since it directly reveals the energy versus momentum information. In this section, I use angle-resolved photoemission as a tool to address the issue of C_{60} band width. The experimental data

from both the normal and off-normal emission were mainly collected along high-symmetry directions.

Figure 4-8 presents two complementary sets of angle-resolved photoemission data from a single crystal of C_{60} cleaved in ultra-high vacuum. Panel (a) gives off-normal emission data with a photon energy of 25 eV, while panel (c) gives normal-emission data at various photon energies. In the normal-emission case, I fixed the direction of the **k** vector but changed its amplitude. In the off-normal emission case, I fixed the amplitude of the **k** vector but changed its direction. In both cases, I change the **k** vector by relatively small amounts. However, this change is very sizable as compared to the small Brillouin zone size of the C_{60} crystal (approximately 60% and 20% for the off- and normal emission cases, respectively) [32]. To first order, the most obvious conclusion from Figure 4-8 is that, although the photoemission feature of C_{60} has a sizable width, there is minimal energy dispersion of the features, i.e., the photoemission features do not move with the change of emission angle or photon energy. The upper boundary for the energy dispersion of the first and second photoemission features is 50 meV, which is shown more clearly in panel (b). We notice that the first photoemission feature (HOMO) shifts by 50 meV at 6° emission angle, and then shifts back by about 20 meV at 9° emission angle. The experimental conditions during the data collection were very stable and I reproduced the normal emission data after I took the off-normal emission data. Therefore, I believe that the experimental observation is real. However, we cannot rule out the possibility that this small shift is caused by a change in the spectral background, or that each photoemission feature contains several states and their relative intensity may change with emission angle and photon energy. In any case, I am confident enough to say that the energy dispersions of the C_{60} photoemission features are very small, and 50 meV is the upper bound.

Hence, our angle-resolved data provide the following picture: although the photoemission feature width is much wider than our experimental resolution, we see neither a sizable energy dispersion nor a sizable change of the photoemission peak width with substantial changes of crystal momentum. This result puts further constraints on the width of the energy bands. The lack of energy dispersion in the photoemission features of this compound does not necessarily mean that there are no dispersions of individual bands. All the photoemission features resolved contain several bands (e.g., the first feature is five fold degenerate), and the individual bands may disperse differently. We might have a situation in which the individual bands have some dispersion while the centroid of these bands is basically non-dispersive. This scenario leads to a change of the width of the photoemission features; however, since I didn't see any sizable changes of the widths of photoemission features, I think the dispersion of individual bands is also small. Another possible explanation for the lack of energy dispersion in our data is the rotational disorder. It is found that the C_{60} molecules spin with high frequencies in the solid [21]. The hopping matrix elements and therefore the band width will be affected by the relative orientations of the C_{60} molecules. Nevertheless, the rotational disorder alone cannot explain why the photoemission features observed are much broader than the instrumentational resolution. A completely disordered system naturally gives narrow bands. Furthermore, since the trend (say, upwards or downwards) of the energy dispersion in C_{60} solid is determined by the crystal structure, the rotational disorder of the individual molecules may produce many bands with different widths but the same trend. We may still see the "averaged energy dispersion" of these bands if some of them are very dispersive. Hence, my data may not be easily explained by rotational disorder alone.

The above discussion makes it very clear that the width of the photoemission feature in C_{60} does not reflect the band width of solid C_{60}. The band width of C_{60} is likely to be much narrower than the width of the photoemission feature, even though it

is difficult to pin down exactly how narrow the real band width is. This assertion is different from an earlier interpretation of the photoemission data [16]. Now the question that must answered is how the broadening of the photoemission peak arises. The instrumentational resolution is not the main cause of the broadening since the typical photoemission experimental resolution is much better than the peak width. Although another traditional cause for a peak broadening is due to the photo-hole lifetime, here we are dealing with either the highest valence band state or the conduction band state, and so the quasi-particles are expected to have a long lifetime. Hence this data cannot be explained by the photo-hole lifetime broadening. The rotational disorder cannot explain it since it naturally gives narrow bands. Thus, other reasons for the broadening of the photoemission spectra must exist.

An important point to remember in interpreting photoemission data is that photoemission is an excited state measurement. Extensive experience, however, shows that photoemission is a very complex process; the spectra even in metals with simple lattice structures exhibit features from not only band type transitions, but also from many other processes. The spectra is further modulated by final state effects and changes in the bulk lattice geometry at and near the surface region. In fact, precedents of final state broadening of photoemission features have been observed in other materials before. For example, the very sharp exciton state of F-centers in KI appeared in the photoelectric emission data to have a width of approximately 1 eV at room temperature [33]. The broadening of the exciton state in F-centers was explained by the Franck-Condon final state effect [34]. Figure 4-9 depicts the photoemission process and the broadening mechanism of the photoemission feature via the Franck-Condon principle. Curves 1 and 2 represent the system energy as a function of some generalized coordinates for the ground state and the excited state, respectively. We start out in the system energy curve 1 with an equilibrium position a_0. In the photoemission process, because of the charge redistribution, the system energy also

has to be changed, and we end up in curve 2. Because the photoemission process is much faster than the speed of the ion movements, all photoemission transitions are vertical transitions. Depending on the shape of curve 2, the spectral width ΔE may be broadened. Such broadening is significant only if there are appreciable changes in the equilibrium positions of the final state. Without an appreciable change of the final state geometry, the optical transition is dominated by the 0-0 transition (n = 0 vibrational state in curve 1 to n = 0 vibrational state in curve 2). If we allow an appreciable change of the geometry in the final state, non 0-0 transitions become possible via the Franck-Condon principle, and they will have significant oscillator strength. These non 0-0 transitions are usually in the steep part of the curve 2, resulting in large ΔE.

One of the most important reasons for such a broadening effect in the F-centers is the localized nature of the system. The photo-hole is local enough so that it makes enough of a change of local geometry, thus the system energy curve as depicted in figure 4-3. Since the photo hole left in the HOMO is distributed in the entire molecule, one would not start out expecting a very large lattice distortion. Although is quite reasonable to believe that the photo-hole is localized within a C_{60} molecule, it is still distributed over 60 carbon atoms. Hence, there is no clear prior reason to believe a large non 0-0 transition in this system. This is consistent with the theoretical calculation that the relaxation energy of the molecule is small [35].

The way one can definitively answer this question is to perform experiments on C_{60} molecules. Fortunately, such studies from gas phase C_{60} have been performed by Lichtenberger *et al* [14] and Baltzer *et al* [36]. These studies show that the photoemission spectra from gas phase are also very broad, and thus unambiguously establish that the photoemission spectra have been broadened by reasons other than energy dispersion. With an exceptionally good energy resolution of 22 meV, Baltzer *et al.* can resolve three features for the highest molecular orbital state (HOMO) [36].

Since HOMO is a mono-energetic state, the three resolved features have to be the vibration states and the non 0-0 transitions have to be strong. Similarly, we expect that vibrational final state effects are important for an understanding of the photoemission data from the solid.

Therefore, we are left with the following picture: the band dispersion in solid C_{60} is quite small, and a significant part of the broadening in the photoemission spectra comes from non 0-0 transitions to excited vibrational final state. This observation provides a possible reason for the bandwidth as determined by photoemission is an order of magnitude larger than that determined by other measurements such as NMR, susceptibility, and IR reflectivity. We suggest that the peak width one measures from photoemission data may be dramatically modified by final state effects, and thus may not reflect the true band width that is substantially narrower.

4.4 Conclusions

In summary, our photoemission spectra from single crystal C_{60} show sharp molecular features, indicating that the molecular orbitals are relatively undisturbed in solid C_{60}. This work observed interesting intensity modulations of the valence band features as a function of the photon energy, indicating strong final state effects. My angle-resolved photoemission data reveals that the C_{60} single crystal has narrow bands that exhibit minimal energy dispersion. I suggest that the band broadening may be caused by the non 0-0 transition to excited vibrational final states. This result reconciles the controversy about the band width of the C_{60} as measured by other techniques.

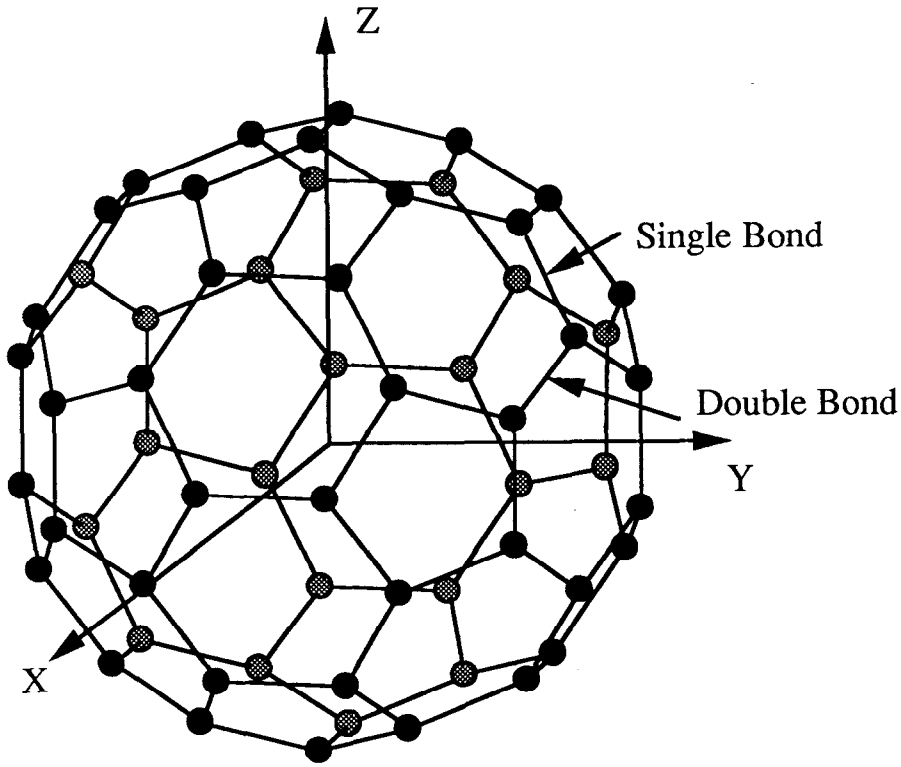

Figure 4-1 Illustration of C_{60} molecular structure. There are two different C-C bonds within the icosahedral symmetry. Single bond is on the regular pentagon (with the length of 1.46Å) and double bond is shared by two hexagons (with the length of 1.40Å).

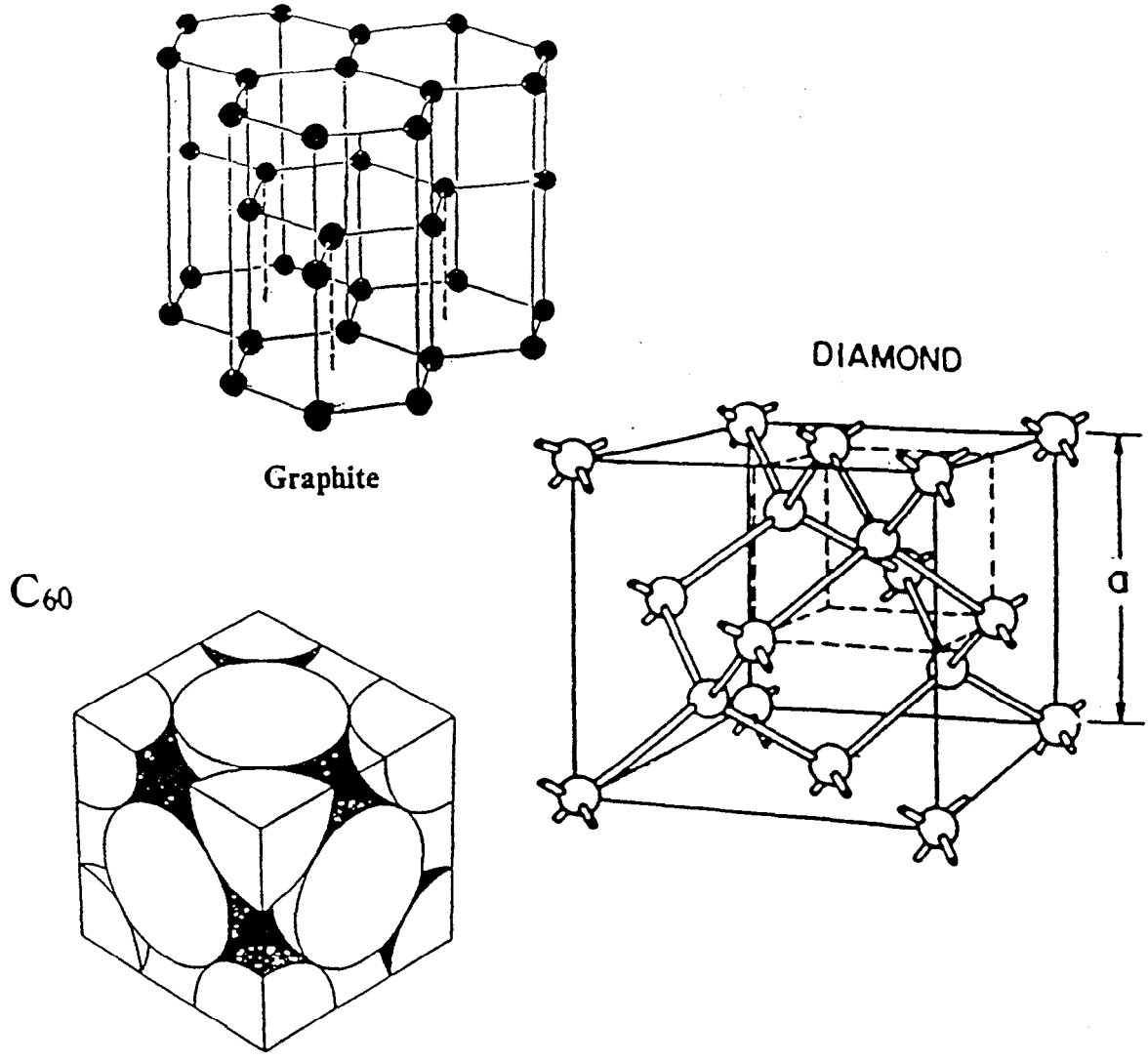

Figure 4-2 Crystal structure of C_{60} together with the crystal structures of other pure forms of carbon: graphite and diamond. Diamond is a tetrahedral coordination of carbon atoms in which each atom is connected to its four nearest neighbors by equivalent sp^3 bonds. Graphite is a highly anisotropic crystal in which three of the carbon valence electrons form sp^2 bonds that link each atom to three neighbors in a hexagonal arrangement within a plane. Adjacent planes are connected by much weaker Van der Waals attractions. For solid C_{60}, within the cage the intramolecular bonds are sp^2 and sp^3 bonds, they are very strong. The C_{60} molecules are bound much less strongly into the crystal lattice by Van der Waals force.

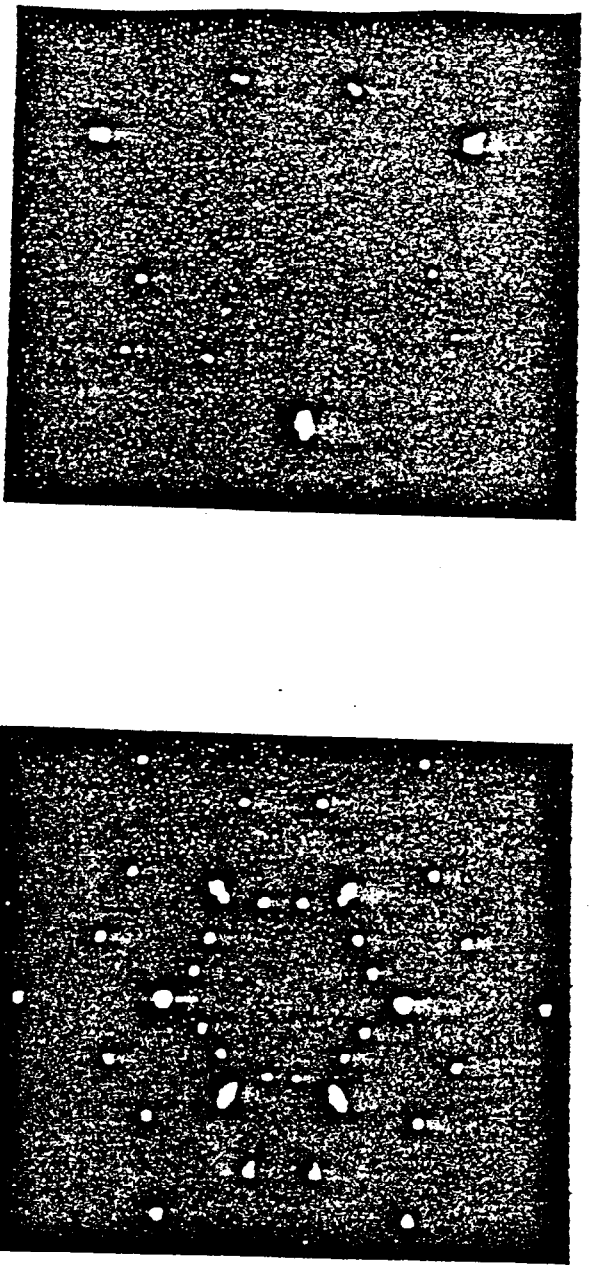

Figure 4-3 Transmission Laue patterns along a cleaved direction of the C_{60} single crystals.

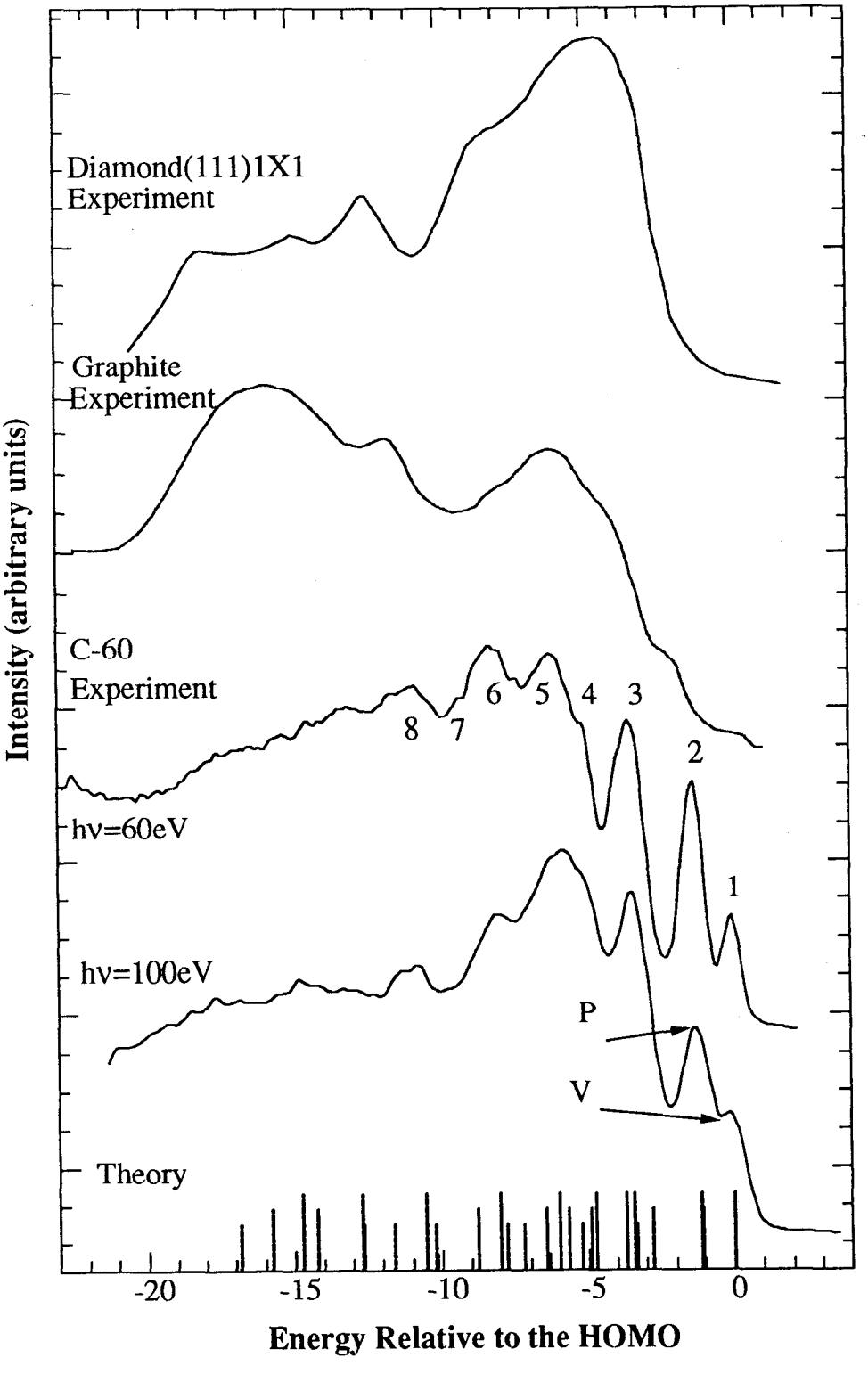

Figure 4-4 Valence band spectra of C_{60} together with that of graphite and diamond.

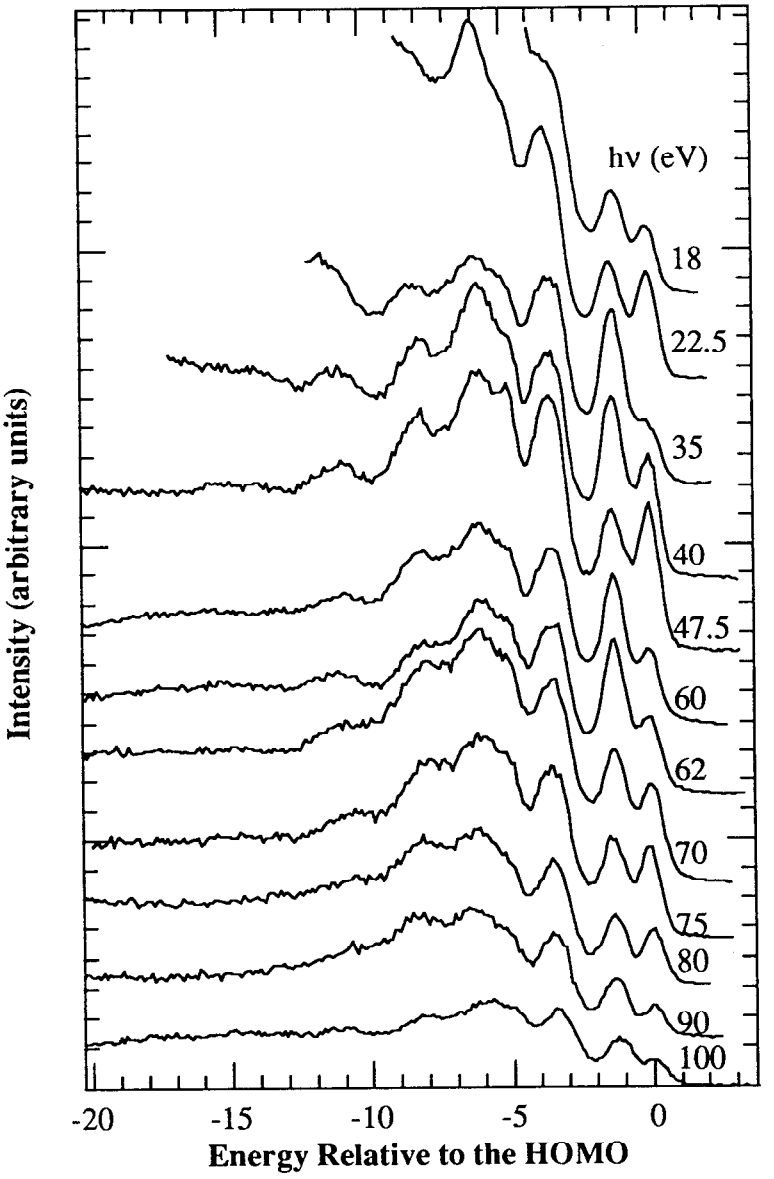

Figure 4-5 Valence band spectra of C_{60} recorded with different photon energies.

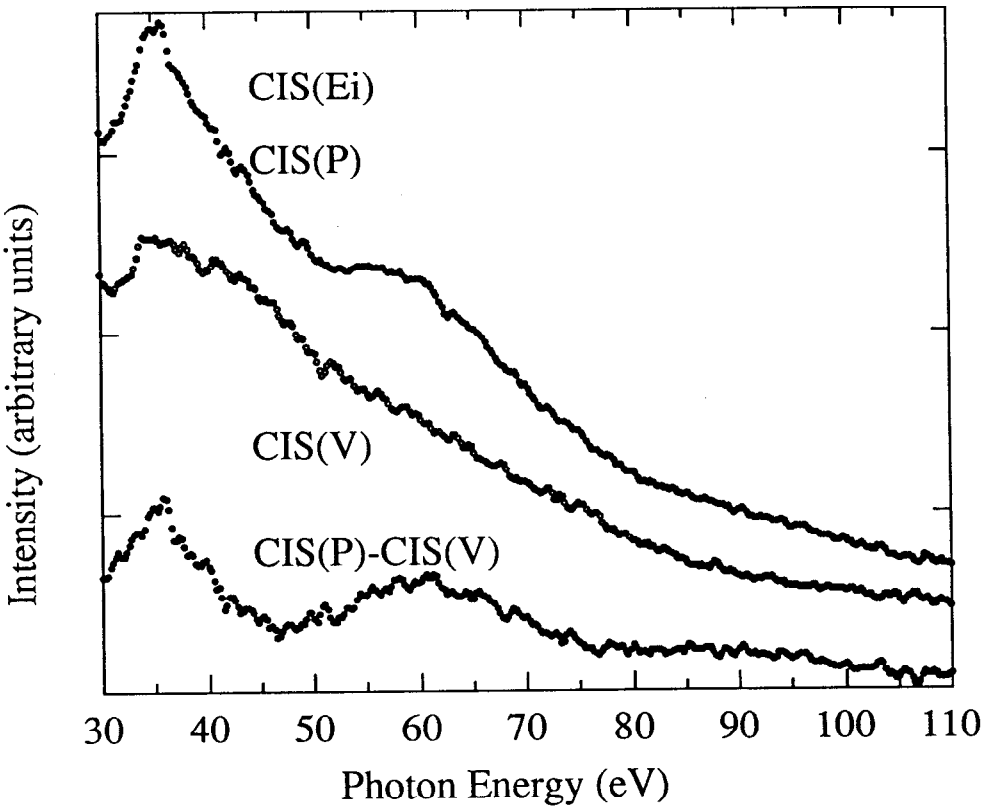

Figure 4-6 Illustration of background subtraction procedure in CIS data.

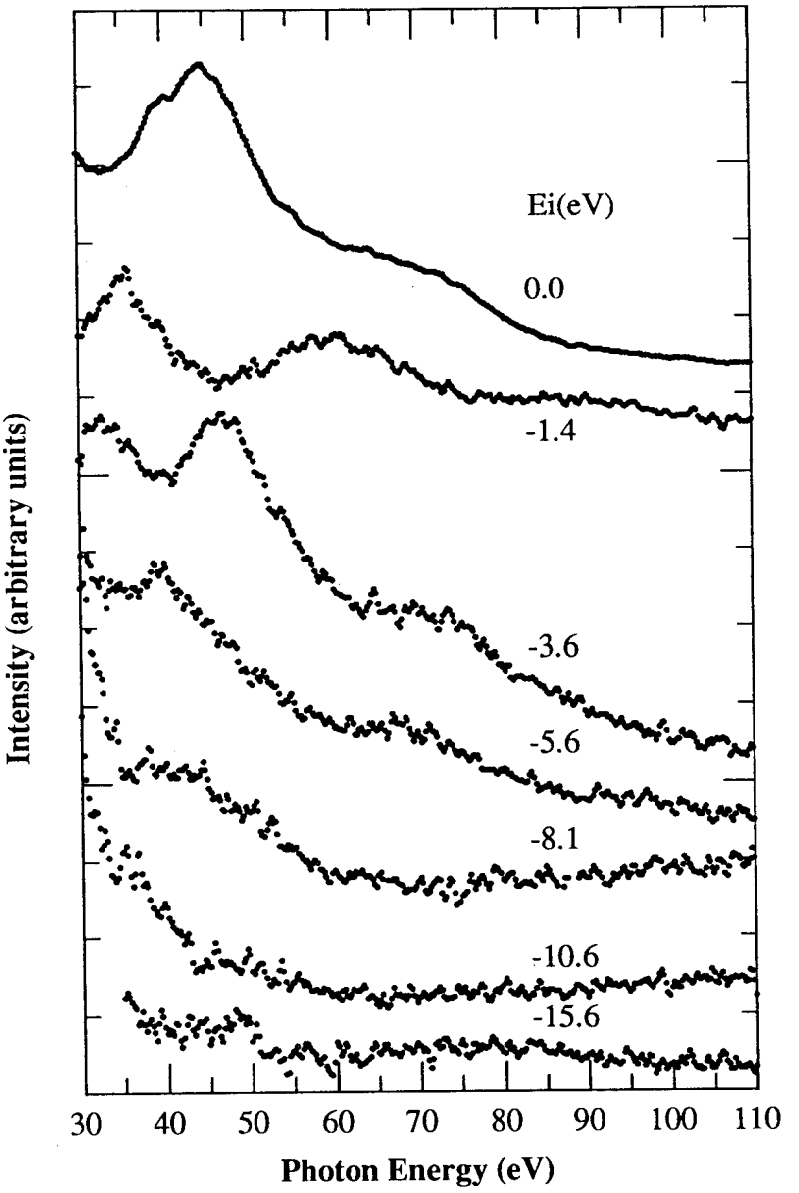

Figure 4-7 CIS spectra with different initial energies corresponding to the peaks in C_{60} valence band spectra.

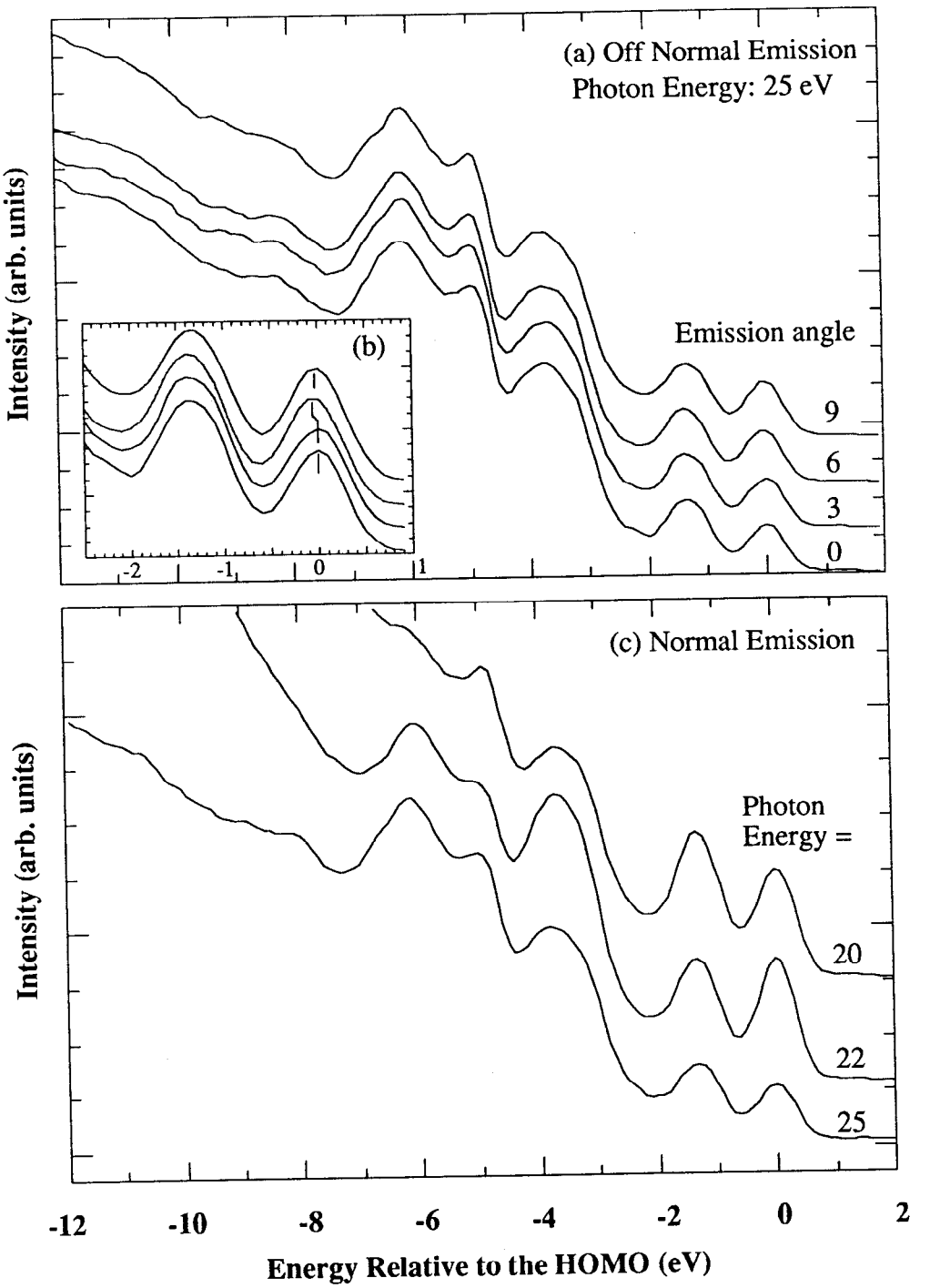

Figure 4-8 (a) Off-normal emission data from the C_{60} single crystal, the inset (b) shows details of the first two photoemission peaks. (c) Normal-emission data from the C_{60} single crystal.

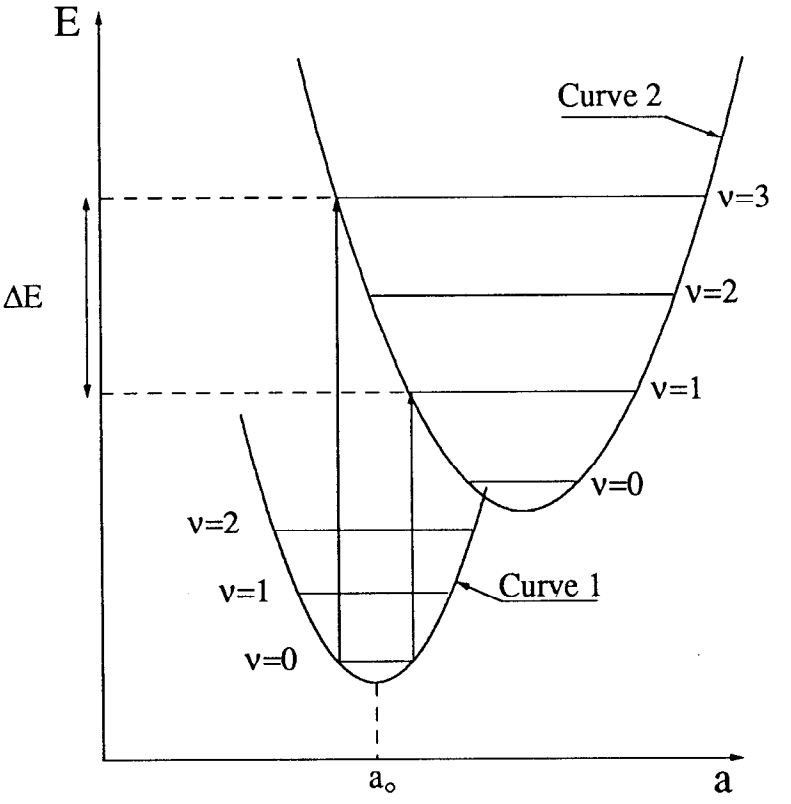

Figure 4-9 Illustration of photoemission process and mechanism of the final state broadening.

References:

1. D. E. H. Jones, New sci. **32**, 245 (1966).
2. E. Osawa, Kagaku, **25**, 854 (in Japanese), (1970).
3. Z. Yoshida, E. Osawa, Aromaticity, Kagakudojin: Kyoto, 1971, pp 174 (in Japanese).
4. H. W. Kroto, J. Heath, S. C. O'Brien, R. F. Curl and R. E. Smalley, Nature **318**, 162 (1985).
5. W. Kräschmer, L. D. Lamb, K. Fostiropoulos, D. R. Huffman, Nature **347**, 354 (1990).
6. Science, **254**, 1534 (1991).
7. A. F. Hebard, M. J. Rosseinsky, R. C. Haddon, D. W. Murphy, S. H. Glarum, T. T. M. Palstra, A. P. Ramirez, A. R. Kortan, Nature **350**, 600 (1991).
8. K. Holczer, O. Klein, S.-M. Huang, R. B. Kaner, K.-J. Fu, R. L. Whetten, F. Diederich, Science **252**, 1154 (1991).
9. K. Holczer, O. Klein, G. Gruner, J. D. Thompson, F. diederich, R. L. Whetten, Phys. Rev. Lett. **67**, 271 (1991).
10. W. J. Blau, H. J. Byrne, D. J. Cardin, T. J. dennis, J. P. Hare, H. W. Kroto, R. Taylor and D. R. M. walton, Phys. Rew. Lett. **67**, 1423 (1991).
10. H. W. Kroto, A. W. Allaf and S. P. Balm, Chem. Rev. **91**, 1213 (1991).
11. R. J. Wilson, G. Meijer, D. S. Bethune, R. D. Johnson, D. D. Chambliss, M. S. De Vries, H. E. Hunziker, H. R. Wendt, Nature **348**, 621 (1990).
12. P. M. Allemand, G. Srdanov, A. Koch, K. Khemani, F. Wudl, J. Am. Chem. Soc. **113**, 2780 (1991).

13. D. L. Lichtenberger, K. W. Nebesny, C. D. Ray, D. R. Huffman and L. D. Lamb, Chem. Phys. Lett. **176**, 203 (1991).

14. J. H. Weaver, J. L. Martins, T. Komeda, Y. Chen, T. R. Ohno, G.H. Kroll, N. Troullier, R. E. Haufler, and R. E. Smalley, Phys. Rev. Lett. **66** 1741 (1991).

15. C. T. Chen, L. H. Tijeng, P. Rudolf, G. Meigs, J. R. Rowe, J. Chen, T. P. McCauley, Jr, A. B. Smith III, A. R. McGhie, W. J. Romanow, and E. W. Plummer, Nature **352**, 603 (1991).

16. G. K. Wertheim, J. E. Rowe, D. N. E. Buchanan, E. E. Chaban, A. F. Hebard, A. R. Kortan, A. V. Makhija, R. C. Haddon, Science **252**, 1420 (1991).

17. T. Takahashi, T. Morikawa, S. Sato, H. K. Yoshida, A. Yuyama, K. Seki, H. Fujimoto, S. Hino, S. Hasegawa, K. Kamiya, H. Inokuchi, K. Kikuchi, Physica C, **185-189**, 417 (1991).

18. S. Saito and A. Oshiyama, Phys. Rev. Lett. **66**, 2637 (1991).

19. Most of reports of C_{60} structure is fcc, e.g., R.M. Flemming et al., Proc. Mater. Res. Soc. (Boston, 1990) in press. However, C_{60} has also been reported to have hcp structure, e.g., W. Kräschmer, L.D. Lamb, K. Fostiropoulos, D.R. Huffman, Nature 347 (1990) 354. We depict the fcc structure here because most of the recent reports give this structure and there are concerns about the impurities in hcp crystals.

20. C. S. Yannoni, R. D. Johnson, G. Meijer, D. S. Bethune, and J. R. Salem, J. Phys. Chem. **95**, 9 (1991).

21. L. D. Rotter et al., preprint.

22. R. Tycko, G. Dabbagh, M. J. Rosseinsky, D. W. Murphy, R. M. Fleming, A. P. Ramirez, J. C. Tully, Science **253**, 884 (1991).

23. A. P. Ramirez, private communication. Susceptibility and critical field measurements also yield a narrow band width (about 7 or 8 times narrower than the photoemission data).

24. D. S. Bethune, G. Meijer, W. C. Tang, H. J. Rosen, W. G. Golden, H. Seki, C. A. Brown, and M. S. de Vries, Chem. Phys. Lett. **179**, 181 (1991).

25. R. Hgeiss, C. H. Brown, O. Chapa-perez, R. J. Savoy, H. R. Wendt, D. Elloway, and M. S. de Vries, to be published.

26. A. Biamoni, S. B. M. Hagstrom and R. Z. Bachrach, Phys. Rev. B **16**, 5543 (1977) .

27. B. B. Pate, Ph.D. Thesis, Stanford University, 1984.

28. G. J. Lapeyre, J. Anderson, P. L. Gobby, J. A. Knapp, Phys. Rev. Lett. **33**, 1290 (1974).

29. P. J. Benning, D. M. Poirier, N. Troullier, J. L. Martins, J. H. Weaver, R. E. Haufler, L. P. F. Chibante, and R. E. Smalley, Phys. Rev. B **44**, 1962 (1991).

30. J. L. Martins, N. Troullier and J. H. Weaver, Chem. Phys. Lett. **180**, 457 (1991).

31. In our estimation, we compared **k** to half of the fcc Brillouin zone since it is symmetric with respect to the zone center. For the normal emission case, an inner potential of 8 eV is used. This approximation will not affect our message that we have covered a sizable portion of the zone. We have additional normal emission data which give the same result.

32. L. Apker and E. Taft, Phys. Rev. **79**, 964 (1959).

33. see, e.g., articles by M. Lax and C. Herring in Photoconductivity Conference, edited by R. G. Breckenridge *et al.*, published by Wiley and Sons.

34. P. Bagus, private communication.

35. P. Baltzer, W. J. Griffiths, A. J. Maxwell, P. A. Brühwiler, L. Karlsson and N. Martensson, to be published.

Chapter 5

Conclusions

5.1 Summary

We have characterized the electronic structure of diamond and C_{60} using angle resolved and core level photoemission.

In the case of the C(100)-(2x1) system, we have studied the C(100)-(2x1) surface electronic structure using both core level and angle resolved valence band photoemission spectroscopy for the first time. One surface component of the C 1s core level spectrum is observed, and it is in agreement with the theoretical calculation that this surface is most likely to consist of only symmetrical dimers. In the valence band spectra we have identified the emission from the surface states and mapped out the dispersion along the [011] /[01$\bar{1}$] directions. The results from this study have been compared with those from the reconstructed Si(100) and Ge(100) surfaces, and we have found that there is a great similarity in the surface electronic structures.

In the case of metal/diamond interfaces, we have performed core level and valence band photoelectron spectroscopy and LEED studies of boron and antimony on diamond (100) and (111) surfaces. Our experimental results show that the B and Sb atoms both bond to the C(100) and C(111) surfaces, and that boron diffuses into the substrate after annealing at 1100°C. The experimental results also reveal that boron and antimony behave very differently on the C(100) and C(111) surface, respectively.

For antimony, upon deposition, only a one-component Sb core level is observed on both the (100) and (111) samples. Upon annealing, the Sb 4d peak at the Sb/C(100) interface broadens slightly and shifts to lower kinetic energy. However, a second component appears in the Sb 4d spectra of the Sb/C(111) sample. For both C(100) and C(111) surfaces, the LEED patterns observed from deposition of one monolayer and subsequent annealing were similar to that of the clean surface.

Although diamond, silicon and germanium are in the same column of the periodic table, the B and Sb atoms act differently on the substrate of diamond than on Si and Ge substrates. We attribute these results to the drastically smaller diamond lattice and the much stronger C-C bond. We also found that desorption of Sb from diamond occurs at a temperature above 1000°C, which indicates that the Sb-C bond is the strongest among Sb-C, Sb-Si and Sb-Ge bonds.

In the case of the single-crystal C_{60}, our photoemission spectra show sharp molecular features, indicating that the molecular orbitals are relatively undisturbed in solid C_{60}. Interesting intensity modulations of the valence band features as a function of the photon energy were observed, indicating strong final state effects. The angle-resolved photoemission data reveal that the C_{60} single crystal has narrow bands that exhibit minimal energy dispersion. We suggest that the band broadening may be caused by the non 0-0 transition to excited vibrational final states. This result reconciles the controversy about the band width of the C_{60} as measured by other techniques.

5.2 Future Work

As the growth methods of diamonds and buckyballs continue to improve, much more work must be carried out to characterize and to understand these processes.

Using photoemission spectroscopy, we have improved our understanding of the electronic structures of diamond surface and metal/C interfaces in this work. However, photoemission spectroscopy has some disadvantages when compared with other techniques, and our understanding of the properties of metal/C interfaces is still quite limited. We should try to exploit the unique advantages of photoemission, and combine the use of other complementary techniques in order to compensate the disadvantages of photoemission.

5.2.1 Clean C Surface

Our preliminary results show the C(100) surface reconstructs to a (2x1) structure. But for the C(100)-(2x1) reconstructed surface, controversy still exists over the proposed structure models. Both monohydride model and π-bond model have the (2x1) LEED symmetry, and hydrogen has been a very difficult adsorbate to detect in the study of solid surfaces. In order to reconcile this controversy, a structure probe, which is sensitive to hydrogen is needed. One way to carry it out is using nuclear reaction analysis (NRA), which is the most reliable experimental techniques for direct determination of absolute hydrogen or deuterium coverages on a surface [1-4].

5.2.2 Metal/C Interface Morphology

The interface structure and stability will be important for almost all applications of diamond. Optical applications will require smooth surfaces and electronic applications will require understanding of Schottky and ohmic metal contacts, and band offsets at semiconducting junctions.

In order to determine the surface geometric and electronic structure of metal/C interfaces completely, we have to use the power of combining several complementary techniques, such as LEED, surface extended X-ray absorption fine structure (SEXAFS), photoelectron diffraction (PD), and photoemission. SEXAFS spectroscopy

has been used as a structural probe since the late seventies [5-7]. It has the ability to measure bond lengths, and coordination numbers and bond angles. PD has by now been developed as a quantitative surface structure probe [8-12]. The use of PD's forward scattering, with very high energy resolution, is a powerful tool in the study of adsorbed molecules, epitaxial overlayers and clean surface. This technique would certainly add furtuer information on the interface structure.

References:

1. R. J. Culbertson, L. C. Feldman, P. J. Silverman, and R. Haight, J. Vac. Sci. Technol. **20**, 868 (1982).
2. T. Nanawa and W. M. Gibson, J. Vac. Sci. Technol. **17**, 256 (1980).
3. Z. H. Lu, K. Griffiths, P. R. Norton, and T. K. Sham, Phys. Rev. B **44**, 5648 (1991).
4. Z. H. Lu, K. Griffiths, P. R. Norton, and T. K. Sham, Phys. Rev. Lett. **68**, 1343 (1992).
5. J. Stöhr, Japan. J. Appl. Phys. **17**, 217 (1978).
6. J. Stöhr, R. Jaeger and S. Brennan, Surf. Sci. **117**, 503, (1982).
7. *Synchrotron Radiation Research*, Edited by H. Winick and S. Doniach, Plenum, New York, 1980.
8. C. S. Fadley, Prog. in Surf. Sci. **16**, 275 (1984).
9. C. S. Fadley, Phys. Scripta **T17**, 39 (1987).
10. S. A.Chambers, Adv. in Phys. **40**, 357 (1990).
11. W. F. Egelhoff, Jr. *Critical Reviews in Solid State and Materials Sciences,* **16**, 213 (1990).
12. C. S. Fadley, *Synchrotron Radiation Research: Advances in surface and Interface Science*, Edited by R. Z. Bachrach, Plenum, New York, 1992.